Ocean Engineering 251 (2022) 111040

Contents lists available at ScienceDirect

Ocean Engineering

journal homepage: www.elsevier.com/locate/oceaneng

Towards the uncertainty quantification of semi-empirical formulas applied to the added resistance of ships in waves of arbitrary heading

Malte Mittendorf [a,*], Ulrik D. Nielsen [a,c], Harry B. Bingham [a], Shukui Liu [b]

[a] DTU Mechanical Engineering, Technical University of Denmark, DK-2800 Kgs. Lyngby, Denmark
[b] School of Mechanical and Aerospace Engineering, Nanyang Technological University, SG-639798 Singapore, Singapore
[c] Centre for Autonomous Marine Operations and Systems, NTNU AMOS, NO-7052 Trondheim, Norway

ARTICLE INFO

Keywords:
Added resistance
Semi-empirical formula
Uncertainty quantification
Parameter calibration
Swarm intelligence algorithm

ABSTRACT

The present paper examines a semi-empirical framework for the estimation of added resistance in arbitrary wave heading under consideration of uncertainty quantification. In this respect, the calibration of the formula's parameter vector is conducted based on particle swarm optimization as well as a database of model test results comprising 25 different ships and around 1100 samples. In the first iteration, the minimization of reducible systematic uncertainty is of interest and the effect of four objective functions on prediction accuracy is evaluated. Moreover, two different parameter combinations were obtained for blunt ($C_B \geq 0.70$) and slender-type ships. Conversely, the irreducible statistical uncertainty, i.e. the inherent noise of the experimental data, is taken into account by a quantile regression procedure. Applying this approach, a 90% prediction interval for the formula's estimates is implemented using the skewed version of the superior loss function in the previous iteration. The practical relevance of an uncertainty estimate for the prediction of the added resistance is emphasized in the final part, in which the proposed approach is validated in regular waves against model test data and other well-established prediction methods. In general, the validation studies suggest satisfactory performance and reliability of the adapted semi-empirical formulation.

1. Introduction

The increasing pressure at societal and legislative levels for the reduction of carbon emissions in the maritime sector makes the accurate and *transparent* prediction of the actual required engine power in realistic seaways an imperative throughout the ship's life cycle. The added resistance is of high relevance in ship design and operation due to its impact on safety and energy efficiency. The decrease in service speed of merchant ships (slow steaming) leads to a larger contribution of the added resistance to the total resistance in relative terms. Thus, the added resistance is mainly a concern for energy efficiency considerations in moderate sea states. In severe sea states, however, the risk of losing maneuverability – for tankers and bulk carriers in particular – is pivotal due to the prevalent trend of reducing installed engine power, in order to comply with the enforced energy efficiency regulations such as the Energy Efficiency Design Index (EEDI), Papanikolaou (2018). This safety concern motivated the legislation of the Minimum Propulsion Power (MPP) regulations by the International Maritime Organization (IMO) for blunt-type ships, in which several semi-empirical formulas are recommended for the practical determination of the added resistance and the associated speed loss in a seaway, cf. IMO (2013, 2016) and IMO (2017).

The numerical calculation of added resistance has attracted much attention over last years using not only potential flow theory methods, such as strip theory (e.g. Amini-Afshar and Bingham (2021)) and panel codes (e.g. Söding et al. (2014)), but also using RANS (Reynolds-Averaged Navier Stokes) methods for calculating the added resistance (e.g. Hizir et al. (2019)), the related propulsive coefficients (e.g. Mikkelsen et al. (2022)) or the maneuvering coefficients (e.g. Uharek (2019)). However, the estimation of hydrodynamic characteristics in waves, such as the added resistance, is subject to large uncertainties both in terms of theoretical/numerical and experimental methods. The SHOPERA (Energy efficient safe SHip OPERAtion) benchmark study, which was part of the eponymous EU-project, revealed remarkable deviations in relatively short wave conditions between numerical results and model test data, cf. Shigunov et al. (2018). As a matter of fact, precisely these conditions (i.e. $\lambda/L_{pp} < 0.5$) are nowadays of high importance according to Kwon (1981) and Minsaas et al. (1983) as ships predominantly sail in these low to moderate sea states. This is a consequence of increasing ship size (economy of scale) and also due to the use of routing optimization/weather routing. Still, short waves impose tremendous challenges on contemporary numerical

* Corresponding author.
E-mail address: mamit@mek.dtu.dk (M. Mittendorf).

https://doi.org/10.1016/j.oceaneng.2022.111040
Received 26 November 2021; Received in revised form 20 January 2022; Accepted 4 March 2022
Available online 23 March 2022

methods and push their applicability towards and beyond the limits. On one hand, the importance of non-linear effects, such as wave breaking in short waves impedes the use of potential flow methods, such as strip theory, for the prediction of added resistance. Additionally, strip theory codes show a lack of accuracy in following and quartering waves, Park et al. (2019). On the other hand, short waves lead to a extremely fine spatial discretization of the free surface requiring immense amounts of computational effort for RANS methods. The computational cost is amplified by the required small timesteps for the temporal discretization, in order to prevent numerical diffusion of the wave elevation ($CFL = \frac{u\Delta t}{\Delta x} < 0.5$ in free surface region), Sigmund (2018).

Despite the increase in the availability of computational resources and the accuracy of high-fidelity Computational Fluid Dynamics (CFD) calculation tools, semi-empirical formulas are still widely applied for the transparent and efficient assessment of a ship's hydrodynamic characteristics in ship design and operation. The development of (semi-)empirical methods for the estimation of the added resistance in waves is a competitive research area and sparked several different studies over the past years. The application cases for such semi-empirical formulas are manifold, e.g. the wave correction during sea trials (Tsujimoto et al., 2021), overall hull and propeller performance monitoring (Taskar and Andersen, 2021) and for bow shape optimization under realistic conditions, Bolbot and Papanikolaou (2016). The bow shape and the stem profile in particular are highly influential on the magnitude of the added resistance. For instance, Yasukawa and Tsujimoto (2020) conducted systematic model tests and showed a significant decrease in added resistance throughout the total range of relative wavelengths for a vertical stem with no protruding bulb compared to a conventional stem geometry with a bulbous bow. In the field of ship operation, the reliable prediction of the added resistance has also considerable influence on routing optimization (weather routing) as well as monitoring the ship technical performance over time and scheduling hull/engine maintenance.

1.1. Literature review

Havelock (1940) pioneered the scientific work of theoretically approximating second order wave forces by deriving a formulation for the steady force acting on vertical circular cylinders. Fujii and Takahashi (1975) proposed their well-renowned formula for the prediction of added resistance caused by diffraction, i.e. wave reflection, by introducing two correction coefficients to Havelock's approach. These two coefficients take forward speed as well as "finite draft" into account and their derivation was based on theoretical results from Ursell and Dean (1947). Takahashi (1988) modified the original formula using model test data. Later, Tsujimoto et al. (2008) and Kuroda et al. (2008) fine-tuned the empirical corrections of the two additional parameters based on experimental data and proposed the so-called NMRI (National Maritime Research Institute Japan) formula. However, Kwon (1981) pointed out that the finite draft influences both the partial reflection effect and energy transmission below the hull. Liu (2020) as well as Mourkogiannis and Liu (2021) proposed a physically more solid semi-empirical formula taking the effects of forward speed, partial reflection and the finite water depth as well as the energy transmission below the hull into account.

In parallel, Jinkine and Ferdinande (1974) proposed an empirical method for the calculation of the added resistance of fast cargo ships due to radiation, i.e. in long waves. The extension of this method for short waves using experimental data resulted in the STAwaveI and STAwaveII formula for the estimation of the added resistance, where the latter was recommended for the use in sea trial corrections by the ITTC (2014). Lang and Mao (2021) proposed a combined approach in their CTH formula (Chalmers Tekniska Högskola) by taking the NMRI formula for short waves and the Jinkine and Ferdinande (1974) approach for long waves. Furthermore, Lang and Mao implemented several correction coefficients in short waves based on experimental data. Faltinsen et al. (1980) developed an analytical asymptotic formula for the calculation of the added resistance in short waves. Kashiwagi et al. (2010) as well as Liu and Papanikolaou (2013) introduced practical corrections for advance speed and short waves, respectively. Just recently, Yang et al. (2018) also modified Faltinsen's asymptotic formula in order to reflect the three following aspects: finite draft, local steady velocity, and the hull shape above the waterline.

Liu et al. (2015), Liu and Papanikolaou (2016) and Liu et al. (2019) established an efficient semi-empirical formula by combining an enhanced version of the work of Jinkine and Ferdinande (1974) in long waves and an adapted version of Faltinsen's asymptotic formula (Faltinsen et al., 1980) in short waves simplified for practical use. Valanto and Hong (2015) show that the added resistance becomes most prominent in bow oblique waves and thus the consideration of heading angles $\beta \neq 180$ deg. is vital for practical application. Hence, the approach for head waves was lately extended to arbitrary heading angles and the proposed approach was validated against a comprehensive database of model test results, Liu and Papanikolaou (2020). Upon successful validation studies, it was recently adopted by ITTC recommended procedure for analyzing sea trial results, ITTC (2021) and Wang et al. (2021). Moreover, the MEPC (Marine Environment Protection Committee) 76 circular (IMO, 2016, 2017, 2021) also endorsed this method for the assessment of the minimum propulsion power of blunt-type ships. Furthermore, Nielsen (2015) and Martinsen (2016) developed the DTU design tool, which is a linear interpolation method aggregating results of three different potential flow theory methods for a wide range of wave headings and hull shapes. Machine Learning (ML) techniques are increasingly employed in the realm of ship hydrodynamics. Thus, Mittendorf et al. (2022) compare Artificial Neural Networks (ANN) and ensemble tree-based methods for the prediction of the added resistance in head to beam waves using the underlying database of the DTU design tool. In addition, Cepowski (2020) proposed another solely data-driven formula by training an ANN on model test data in head wave conditions and extracted the corresponding equation from the obtained model parameters and activations.

One can conclude that (semi-)empirical methods for the estimation of the added resistance in waves have evolved over time. The mathematical frameworks underwent multiple iterations and experienced an increase in accuracy as more model test data became available and as data analysis methods became more advanced. Holt and Nielsen (2021) assessed the recently passed MPP regulations using empirical methods for the estimation of added resistance. Their study sparked the idea of the present contribution in adapting the longitudinal radius of gyration k_{yy} for the increase in prediction accuracy of the STAwaveII formula. Just recently, Gatchell (2018) presented a parameter calibration of the Hollenbach (1998) calm water resistance estimation method for contemporary RoPax hull shapes using CFD results and Particle Swarm Optimization (PSO). Nikolopoulos and Boulougouris (2019) on the other hand employed the multi-objective genetic algorithm NSGA-II (Non-dominated Sorting Genetic Algorithm) to adapt the Holtrop and Mennen (1982) framework statistically for blunt ships using model test data. Moreover, they expressed the uncertainty for each prediction *quantitatively* by an analytical equation. Lastly, the rigorous parameter calibration as well as uncertainty quantification are still unexplored in the field of added resistance, and hence represent the novelties of the following contribution.

1.2. Motivation and objective

The majority of estimation methods for the added resistance in waves only consider head waves and provide deterministic predictions showing severe practical limitations for these established formulas. In this work, however, we make use of the formulation of Liu and Papanikolaou (2020) for arbitrary wave heading and attempt to minimize the reducible uncertainty pertaining the estimation of the added

resistance and express the irreducible component *quantitatively*. Quoting the famous aphorism of George Box,[1] it is the overall aim of this paper to enhance the usefulness of the semi-empirical formula of Liu and Papanikolaou (2020) and accompany the estimates with uncertainty bounds. In essence, the presented approach combines the transparency of a simple semi-empirical formula with the accuracy and predictive power of a supervised machine learning method in a multivariate regression context. This will be addressed in two stages: (1) In the *holistic* parameter calibration or rather training procedure a metaheuristic optimization algorithm and a dataset of benchmark model test results are employed. The parameter vector will be adjusted minimizing, and comparing several different loss functions. (2) In the second iteration, new parameters are derived using a quantile loss function for lower and upper bounds establishing a 90% prediction interval. The resulting framework is comparable to the method of Hollenbach (1998) which provides lower and upper bounds, along with the actual prediction, for the estimation of the calm water resistance. Furthermore, it is envisioned to provide a pseudo-stochastic prediction of the added resistance for arbitrary heading instead of a deterministic one as a trustworthy representation of uncertainty is an imperative in safety-critical domains such as wave loads on ships.

1.3. Composition

In the following Section 2, the analysis of the used database and the residual analysis of the underlying (Liu and Papanikolaou, 2020) formula will be presented. Section 3 is devoted to elucidate the applied calibration methodology and presents the adapted and parameterized semi-empirical formulation as well as the particle swarm optimizer. Section 4 provides the obtained results and discussion, which includes the validation in regular waves investigating a number of case studies. In the final Section 5, conclusions are drawn and suggestions for extending the work are presented.

2. Data analysis

Experiments on added resistance started in the 1960s and were exploited to gain understanding of the behavior and performance of ships in a realistic seaway as well as for the validation of numerical and empirical tools. Conducting this kind of experiments requires highly accurate measurement equipment, as the added resistance is a higher order force and in most cases only of small magnitude compared to the calm water resistance. In general, the added resistance is seen as a *non-viscous* phenomenon and can be obtained from the square of ship-generated waves, consisting of a linear superposition of diffraction and radiation waves. Kashiwagi (2013) shows that the diffraction component is not frequency dependent and nearly constant throughout the entire regime of wavelengths. Initially, this may seem contradictory, however, Kashiwagi et al. (2010) conclude from experimental data in head wave conditions that the radiation component takes negative values in longer waves due to the interaction terms. Thus, the sum of both contributions yield small, but positive values approaching zero with increasing relative wavelength. The radiation component is, in fact, frequency dependent and dominant in long to medium wavelengths. On the other hand, the diffraction part is relatively more pronounced in shorter waves. Blok (1993) splits the contributions to the added resistance into (1) operational conditions, i.e. wavelength λ, amplitude ζ_a and relative heading β as well as ship speed Fn and (2) driving factors related to the ship, i.e. main particulars and hull shape.

Table 1 presents an array of experimental data for head, oblique and following waves and represents the employed database of this work. The main particulars of the examined ships are indicated and also the references are given in Table 1. It is stressed that only realistic ship designs are taken into account and mathematical hull definitions, such as the Wigley hull, are disregarded due to the missing similarity to contemporary hull forms. The database is characterized by $L_{pp} \in [90, 355]$m, $C_B \in [0.503, 0.858]$ and $Fn \in [0.0, 0.3]$. According to Papanikolaou (2014), the L/B and B/T ratios resemble the current world fleet only to some extent: The L/B ratios show small variation $L/B \in [5.05, 7.5]$ compared to $L/B \in [4.5, 8.5]$ for the world fleet. (2) The B/T ratios are slightly higher than the values of the current world fleet with $B/T \in [2.5, 4.7]$ compared to $B/T \in [2.1, 4.0]$. The mentioned deviations are the first indications for systematic or rather *epistemic* uncertainty of the available data. The decomposition of the database regarding ship type is presented in Fig. 1(a) and reveals only minor deviations to the current (2019) composition of the world fleet according to gross tonnage, cf. Equasis (2019). However, general cargo ships are over-represented in the present database comparing 24% to only 4.5% in reality. In addition, the corresponding number of bulk carriers is too small comparing 16% to 34% for the world fleet as of 2019.

The uncertainty of the added resistance in seafaring conditions is a well-known problem, but is despite its relevance, not well studied. Park et al. (2015) provide uncertainty sources of respective model tests and Papanikolaou and Liu (2021) address this problem qualitatively. Initially, two uncertainty categories are introduced: (A) *Epistemic* or systematic uncertainty results from limitations of the available data, i.e. missing observations. For instance, in short waves ($\lambda/L_{pp} < 0.5$) and non-head wave conditions considerable epistemic uncertainty is present. The database consists of 1127 samples of 25 ships in total, but for $\beta < 180$ deg. only 470 samples are included corresponding to 42% of the total number of samples, whereas the sample size for $\lambda/L_{pp} < 0.5$ is even smaller at 231, cf. Fig. 1(b). (B) *Aleatoric* or statistical uncertainty on the other hand, is due to the stochastic (non-deterministic) character of the observations themselves and is thus an inherent part of the data. Hence, the aleatoric uncertainty does not decrease by increasing the sample size of the model test results. Soize (2017) and Hüllermeier and Waegeman (2021) provide comprehensive overviews of uncertainty quantification and the distinction of uncertainty components.

Park et al. (2015) list five sources of aleatoric uncertainty regarding experiments for the added resistance: (1) Instrument uncertainty, (2) mass distribution uncertainty, (3) calibration uncertainty, (4) measurement uncertainty and (5) data reduction uncertainty. Papanikolaou and Liu (2021) also highlight the uncertain influence of wave steepness on data quality in short waves as well as limitations of towing tanks for measuring the added resistance in short and especially oblique as well as following waves due to, for example, wall effects, such as reflection. Finally, experiments pertaining the added resistance are carried out under partial dynamic similarity, i.e. constant Froude number. Thus, viscous forces are, in fact, relatively more pronounced than in full scale, which might also introduce additional uncertainty in short waves.

Conducting residual analysis of the original approach of Liu and Papanikolaou (2020), it is observed that the residual variance not only increases with the magnitude of the added resistance coefficient, but also with increasing forward speed (Fn). This phenomenon is known as heteroskedasticity, i.e. the variance growth with an increase of a target variable. The well-established p-test of Breusch and Pagan (1979) identifies, whether regression models exhibit heteroskedastic residuals and violate the normality of the residuals and thus the assumption of linear regression. If the test statistics have a p-value below a sensible threshold (e.g. $p < 0.05$), the null hypothesis H_0 of homoskedasticity is rejected. The residuals of the Liu and Papanikolaou formula resulting from application to the present dataset have a p-value of $p \ll 0.05$, which proves heteroskedasticity. In the following parameter calibration we attempt to reduce the degree of heteroskedasticity. Furthermore, the residual analysis revealed a structural break at $C_B = 0.70$, which is reflected in the experimental data of the bluntness coefficient B_f of the original NMRI formula, cf. Fig. 6 in Liu and Papanikolaou (2016).

[1] "All models are wrong, but some are useful".

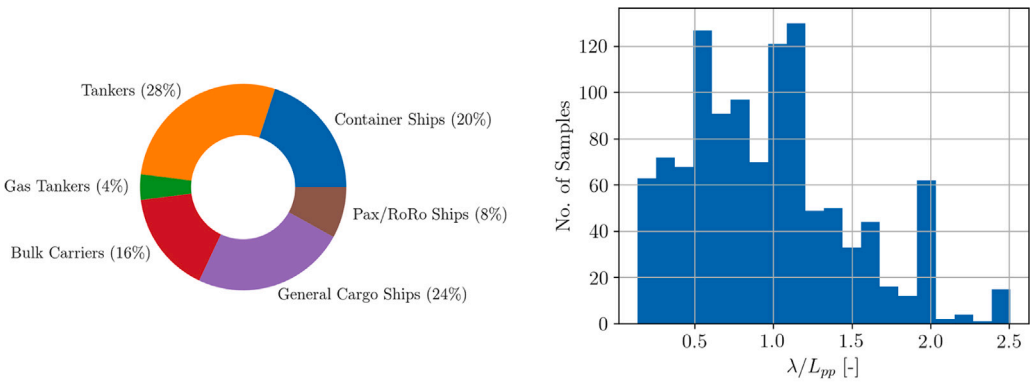

(a) (b)

Fig. 1. Breakdown per ship type (a) and relative wavelength (b).

Table 1
Database of benchmark model test data.

Ship	L_{pp} [m]	B [m]	T [m]	C_B [–]	Fn [–]	β [deg.]	Reference
170BC	279	45	16.5	0.858	0.128	{180,150,120, 90,60,30,0}	Kashiwagi et al. (2004)
DTC	355	51	14.5	0.661	{0.0,0.052,0.139}	{180,150,120, 90,60,30,0}	Shigunov et al. (2018) and Sprenger et al. (2017)
HSVA cruise ship	220.27	32.04	7.2	0.654	0.233	{180,150,120, 90,60,30,0}	Valanto and Hong (2015)
KCS	230	32.2	10.8	0.651	0.26	{180,90,0}	Simonsen et al. (2014) and Stocker (2016)
KVLCC2	320	58	20.8	0.808	{0.0,0.055,0.11,0.142}	{180,150,120, 90,60,30,0}	Shigunov et al. (2018), Guo and Steen (2010) and Sadat-Hosseini et al. (2013)
S175	175	25.4	9.5	0.572	{0.15,0.2,0.25,0.3}	{180,150,120, 90,60,30,0}	Fujii and Takahashi (1975) and Nakamura and Naito (1977)
S-Cb84	178	32.26	11.57	0.84	{0.0,0.048,0.099,0.166}	{180,150, 90,30}	Yasukawa et al. (2019)
S-LNGC	290	45	11.5	0.79	0.19	{180,150,120, 60,30,0}	Kim et al. (2021)
SNU tanker	323	60.0	21.0	0.83	0.137	{180,150,120, 90,60,30,0}	Park et al. (2019)
Aframax tanker	239	44	13.6	0.835	0.154	180	Oh et al. (2015)
Bulk carrier	285	50	18.5	0.829	{0.0,0.05,0.1,0.15}	180	Kadomatsu et al. (1989)
Container ship	300	40	14	0.66	0.247	180	Tsujimoto et al. (2008)
Product carrier	145.4	23.4	8	0.757	0.177	180	Li et al. (2016)
S.A. van der Stel	152.5	22.8	9.14	0.563	{0.15,0.2,0.25,0.3}	180	Gerritsma and Beukelman (1972)
			5.2	0.503	{0.15,0.2,0.25,0.3}	180	Gerritsma and Beukelman (1972)
RIOS bulker	2.0	0.333	0.107	0.8	0.18	180	Kashiwagi et al. (2019)
RoPax	90	17.82	4.2	0.549	0.087	180	Sprenger et al. (2015)
Series 60 ($C_B = 0.6$)	121.96	16.254	6.492	0.6	{0.266,0.283}	180	Strøm-Tejsen et al. (1973)
Series 60 ($C_B = 0.65$)	121.96	16.816	6.73	0.65	{0.237, 0.254}	180	Strøm-Tejsen et al. (1973)
Series 60 ($C_B = 0.7$)	121.96	17.42	6.79	0.7	{0.207,0.222}	180	Strøm-Tejsen et al. (1973)
Series 60 ($C_B = 0.75$)	121.96	18.062	7.22	0.75	{0.177,0.195}	180	Strøm-Tejsen et al. (1973)
Series 60 ($C_B = 0.8$)	121.96	18.757	7.495	0.8	{0.147,0.165}	180	Strøm-Tejsen et al. (1973)
SR221C tanker	320	58	19.3	0.803	0.15	180	Kashiwagi et al. (2004)
Supramax tanker	192	36	11.2	0.84	0.17	180	Yu et al. (2017)
ULYSSES tanker	187.3	32	12	0.82	{0.06,0.12,0.17}	180	SSPA (2012)
WILS II container ship	324	48.4	15	0.602	0.183	180	Söding et al. (2014)

This structural break is highlighted in Fig. 2, in which the residuals are presented for the block coefficient C_B and the Froude number Fn.

It is assumed that the variance increase with higher forward speed is the same as for slender ships (i.e. $C_B < 0.70$) since they usually operate under higher speeds compared to more full-type vessels. In fact, they are subsequently also experimentally examined at these relatively high speeds. Furthermore, the residuals are reasonably balanced for $C_B \geq 0.70$, whereas the formula provides in general too small values for slender ships. The biased residuals for the fast and fine ships strongly motivates splitting the database at $C_B = 0.70$ and obtaining two separate updated parameter vectors for the Liu and Papanikolaou (2020) method. The resulting two datasets are presented in Fig. 3 and comprise 598 for $C_B \geq 0.70$ and 529 samples for $C_B < 0.70$.

It is appreciated that not only the residuals, but also the slender ships' added resistance coefficients are characterized by larger variance compared to the corresponding values of the blunt-type ships. Moreover, it is obvious that the database is biased (unbalanced) towards head wave conditions and relative wavelengths $\lambda/L_{pp} \leq 1.0$, cf. Fig. 1(b). In addition, the dataset for the full-type ships is slightly larger, but in general the database is considered as sufficiently balanced. Furthermore, it is apparent in Fig. 3 (mainly in (a)) that the maximum of the non-dimensional added resistance in head waves appears at a slightly larger wavelength than ship length and reaches zero asymptotically for wavelengths larger than twice the ship's length. Two possible reasons leading to the notable variance in head wave conditions may be attributed to inaccuracies in the experimental setup and the use of

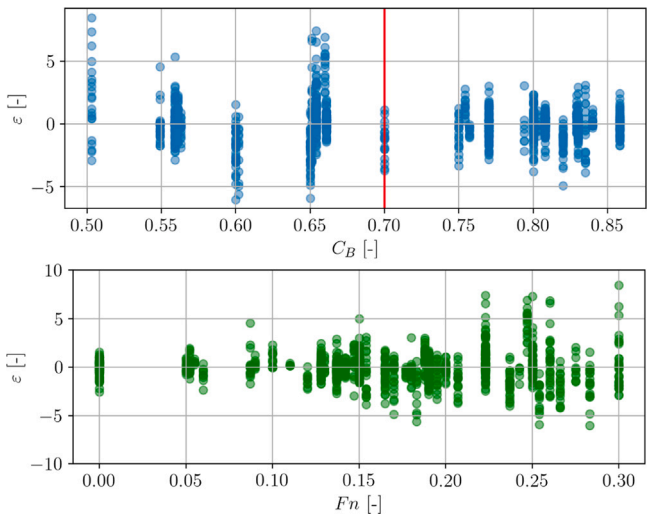

Fig. 2. Residual analysis ε for block coefficient C_B and Froude number Fn. It is noted that the residuals are defined as $\varepsilon_i = y_i - \hat{y}_i$, where y_i is considered as the ground truth.

different wave amplitudes and thus wave steepnesses. Additionally, the incident wave amplitude ζ_a is neither spatially nor temporally constant in a towing tank (not even in one run of experiments). Since, the added resistance is proportional to ζ_a^2, spatio-temporal uncertainty of ζ_a leads to large scatter or rather aleatoric uncertainty. The attributed scatter vanishes when normalizing the experimental data with the measured ζ_a^2, which is also indicated by Maruo (1957). Another reason for uncertainty might be different natural frequencies in heave as well as pitch due to different advance speeds. Despite the theory of Faltinsen's asymptotic formula, the non-dimensional added resistance is trivially zero for $\lambda/L_{pp} = 0.0$. In short waves, the non-dimensional added resistance reaches nearly a constant value, but in some cases tends towards large magnitude and variance, which is partly owed to wave breaking effects at the bow. The latter phenomenon is presumably attributed to relatively high wave steepnesses H/λ, as Park et al. (2015) pointed out. Sigmund (2018) comes to the same conclusion by comparing three different wave steepnesses and their influence on the non-dimensional added resistance by conducting RANS simulations. It was found that increasing the wave steepness in turn slightly decreases the magnitude of C_{AW} in long waves and increases C_{AW} in non-linear fashion in short waves. It is thought that all experiments were carried out with different wave steepnesses, but more importantly under relatively large (and varying) wave amplitudes ζ_a magnifying small added resistance values in order to be measured sufficiently. Unfortunately, it is not possible to study the dependency of the residuals on the wave steepness or wave amplitude as most publications do not specify these values. Moreover, the influence of forward speed $Fn \neq 0$ and non-linear effects, such as wave breaking, contribute to the increase of C_{AW} in relatively short waves. Ultimately, the added resistance is largest in head to beam waves and only of comparably small magnitude in beam to following seas. Hence, the DTU design tool (cf. Nielsen (2015) and Martinsen (2016)) and the NMRI formula (cf. Tsujimoto et al. (2008)) assume the added resistance in waves to be equal to zero for the latter range of wave headings as it is thought that the degree of uncertainty exceeds the actual magnitude of the wave-added resistance. However, the adoption of semi-empirical formulas for the prediction of added resistance depends on the appropriate representation of physical phenomena including the possibility of estimating a negative value like the wave drift force in following waves. Therefore, the presented approach imposes no restrictions of the considered relative wave heading angle β.

3. Applied methodology

The present parameter calibration procedure requires the minimization of one objective, or rather loss, function $\mathfrak{L}$ which is subject to the parameter vector x_i and independent variables θ_m. This methodology can be expressed mathematically as: $\min \mathfrak{L}(x_i|\theta_m)$. Herein, the metaheuristic Particle Swarm Optimization (PSO) algorithm is applied for finding the global minimum due to the highly discontinuous and scattered loss landscape, i.e. without a smooth gradient. The randomized, population-based PSO method was proposed by Kennedy and Eberhart (1995) and mimics the social behavior of bird or fish swarms. Each particle is characterized by a position vector $x_i = [x_1, x_2, \ldots, x_n]^T$ in the n-dimensional search space $\Omega \subseteq \mathbb{R}^n$ and a corresponding velocity vector v_i.

$$v_j^{k+1} = \Phi v_j^k + c_1 r_1 (P_j^k - x_j^k) + c_2 r_2 (G_j^k - x_j^k) \tag{1}$$

In Eq. (1), j denotes the jth particle and k is the iteration index. Moreover, Φ is the inertia weight or the momentum term, whereas c_1 and c_2 are two strictly positive weights for balancing the exploitation of P_j^k and G_j^k – the particle's best and the global best parameter combination, respectively. The social behavior is implemented using the globally or locally best solutions and c_1 and c_2 are considered as cognitive and social impact, respectively. Hence, the choice of the c_1 and c_2 coefficients is of high importance for the PSO algorithm performing well throughout the optimization procedure. On the other hand, r_1 and r_2 are two random variables drawn from a uniform distribution between 0 and 1. The velocity update of the parameter vector x_j^{k+1} is defined in Eq. (2).

$$x_j^{k+1} = x_j^k + v_j^{k+1}. \tag{2}$$

As has been described, balancing the cognitive and social impact coefficients is decisive for the convergence of the optimization procedure. Therefore, the *adaptive* PSO algorithm proposed by Zhan et al. (2009) is applied in the present work. Ultimately, it suffices to specify initial values for Φ, c_1 and c_2, and after each iteration the corresponding values are changed dynamically. The updated values are determined by the spread from the global optimum. In the present paper, the implementation of the Python software package *Pymoo* developed by Blank and Deb (2020) is employed and we choose the following initial values: $\Phi = 0.9$, $c_1 = 2.0$ and $c_2 = 2.0$. Moreover, an upper velocity bound is enforced in order to prevent the rapid movement of particles in the search space Ω, and the corresponding value is defined as $v_{max} = 0.025$. The population size is 25 and termination criteria are the following: (1) The threshold of the change of objective function is set to 10^{-6} and (2) the maximum number of generations is 10^5. Moreover, the initial solutions are not drawn randomly, but by Latin Hypercube Sampling which is a stratified sampling technique proposed by McKay et al. (1979). The computations were performed on an Intel© Core™ i7-8565U CPU, 1.80 GHz with 16 GB physical memory (RAM).

3.1. Adapted semi-empirical framework

The mathematical framework for the prediction of the added resistance R_{AW} combines a variation of the empirical approach of Jinkine and Ferdinande (1974) for long waves and a simplified version of Faltinsen's asymptotic formula in the short wavelength regime . Further simplifications and empirical regression coefficients were introduced, Liu et al. (2015). The original approach originated in the SHOPERA EU-project which addressed the rational calculation of the hydrodynamic behavior of ships in waves. In the present paper, we make use of the latest version of this method which imposes no restrictions on the wave heading, Liu and Papanikolaou (2020). The input vector to the formula is the following $\theta_m = [\lambda, L_{pp}, B, T_f, T_a, C_B, L_E, L_R, \beta, k_{yy}, Fn]^T$. It is noted that T_a and T_f denote the draft at in aft and forward position, respectively. Moreover, L_E and L_R are the lengths of entrance and describe the length between the fore- and aft-most position to the start

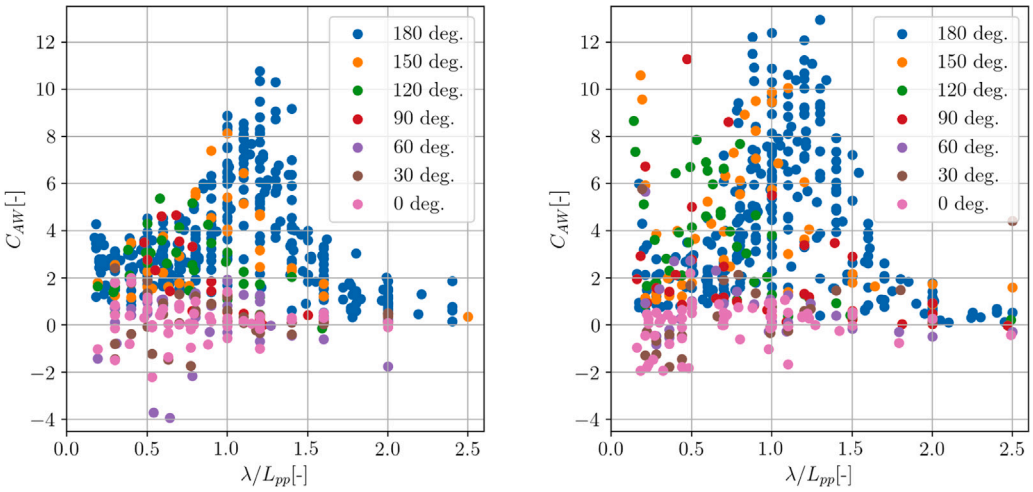

(a) $C_B \geq 0.70$ dataset with 598 samples. (b) $C_B < 0.70$ dataset with 529 samples.

Fig. 3. Samples of the C_{AW} database. (For interpretation of the references to color in this figure legend, the reader is referred to the web version of this article.)

and end of the parallel midship body. The parameter vector x_i comprises 29 constants of the initial formulation by Liu and Papanikolaou (2020), which are presented in Table 2 alongside the corresponding updated values. It is stressed that the signs of the parameters are not changed and only strictly positive values are considered in the parameter (or position) vector x_i. For detailed information and guiding sketches, cf. Liu and Papanikolaou (2020). In contrast to the original paper, we present the non-dimensional added resistance coefficient C_{AW}, cf. Eq. (3).

$$C_{AW} = \frac{R_{AW} L_{pp}}{\rho g \zeta_a^2 B^2} \tag{3}$$

It is noted that g denotes the gravity acceleration and ρ reflects the sea water density. In this work, the non-dimensional added resistance coefficient C_{AW} is decomposed into (1) a base term $C_{AW,M}$ resulting from ship motion and (2) a residual term for bow reflection $C_{AW,R}$ due to diffraction in short waves. The latter contribution is considered as a practical correction as the method by Jinkine and Ferdinande (1974) shows only satisfactory accuracy in medium to long waves. A similar correction approach is described by Tsujimoto et al. (2008). Following the approach of Liu and Papanikolaou (2020), the reflection contribution is calculated using a modified version of Faltinsen's formula and takes the following form.

$$C_{AW,R} = \sum_{i=1}^{4} C^i_{AW,R}. \tag{4}$$

The reflection component is expressed in Eq. (4) separately for each of the four segments S_i. Note that S_1 and S_2 are the port and starboard parts of the bow, whereas S_3 and S_4 are the port and starboard parts of the stern part, respectively.

$$C^1_{AW,R} = x_2 \frac{L_{pp}}{B} \alpha_{T*} \left\{ \sin^2(E_1 - \beta) + \frac{2\omega_0 U}{g} \times [\cos E_1 \cos(E_1 - \beta) - \cos\beta] \right\} \left(\frac{0.87}{C_B} \right)^{(1+4\sqrt{Fn})f(\beta)} \tag{5}$$

$$C^2_{AW,R} = x_2 \frac{L_{pp}}{B} \alpha_{T*} \left\{ \sin^2(E_1 + \beta) + \frac{2\omega_0 U}{g} \times [\cos E_1 \cos(E_1 + \beta) - \cos\beta] \right\} \left(\frac{0.87}{C_B} \right)^{(1+4\sqrt{Fn})f(\beta)} \tag{6}$$

We note that ω_0 is the intrinsic wave frequency, the ship's advance speed is denoted with U in [m/s] and α_{T*} is the draft coefficient which will be defined at a later stage. The form factor $\left(\frac{0.87}{C_B}\right)^{(1+4\sqrt{Fn})f(\beta)}$, which accounts for non-linear effects induced by the fore shoulder, is neglected (i.e. equal to 1) in following wave conditions (cf. Eqs. (7) & (8)) and not considered in the parameter calibration as its modification affected convergence behavior negatively.

$$C^3_{AW,R} = -x_2 \frac{L_{pp}}{B} \alpha_{T*} \times \left\{ \sin^2(E_2 + \beta) + \frac{2\omega_0 U}{g} [\cos E_2 \cos(E_2 + \beta) - \cos\beta] \right\} \tag{7}$$

$$C^4_{AW,R} = -x_2 \frac{L_{pp}}{B} \alpha_{T*} \times \left\{ \sin^2(E_2 - \beta) + \frac{2\omega_0 U}{g} [\cos E_2 \cos(E_2 - \beta) - \cos\beta] \right\} \tag{8}$$

It is stressed that C^1_{AWR} is valid for $E_1 \leq \beta \leq \pi$, C^2_{AWR} in $\pi - E_1 \leq \beta \leq \pi$, $C^3_{AW,R}$ is valid for angles in $0 \leq \beta \leq \pi - E_2$ and C^4_{AWR} is defined for $0 \leq \beta \leq E_2$. Both E_1 and E_2 are considered as entrance angles of the aft and bow part of the ship of interest.

$$E_1 = \arctan\left(\frac{0.99 \cdot B/2}{L_E} \right) \tag{9}$$

$$E_2 = \arctan\left(\frac{0.99 \cdot B/2}{L_R} \right) \tag{10}$$

The non-dimensional added resistance due to motion is calculated in the following way using several regression coefficients:

$$C_{AW,M} = x_1 a_1 a_2 a_3 \bar{\omega}^{b_1} e^{\frac{b_1}{d_1}(1-\bar{\omega}_1^d).} \tag{11}$$

In the following, the heading dependent regression coefficient a_1 for the calculation of the motion component $C_{AW,M}$ is presented.

$$a_1 = \begin{cases} x_3 C_B^{x_4} (x_5 k_{yy})^2 \left(\frac{x_6}{C_B}\right)^{-(1+Fn)\cos\beta} \left(\ln \frac{B}{T_{max}}\right)^{-1} \frac{(1-2\cos\beta)}{x_7} & \text{for } \beta \in [\frac{\pi}{2}, \pi] \\ \text{linear interpolation between } \beta = \pi/2 \text{ and } \beta = 0 & \text{for } \beta \in]0, \frac{\pi}{2}[\\ f(U, V_g) & \text{for } \beta = 0 \end{cases} \tag{12}$$

The coefficient a_1 requires special attention in beam to following waves and its determination is described briefly in the next paragraph. For elaborate explanations and the theoretical derivation consult the original paper of Liu and Papanikolaou (2020).

The calculation of a_1 in stern oblique waves $\beta \in]0, 90[$ deg. is performed by linear interpolation between the beam and following

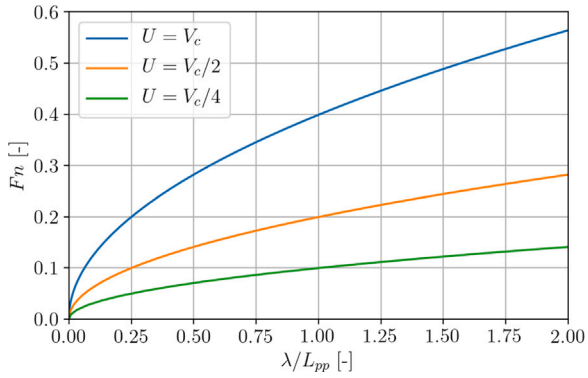

Fig. 4. Ship forward-speed for which the maximum added resistance changes its sign dependent on the relative wavelength, according to Liu and Papanikolaou (2020). (For interpretation of the references to color in this figure legend, the reader is referred to the web version of this article.)

sea case. The coefficient a_1 in following waves is highly dependent on the wave's phase velocity V_c as well as the ship advance speed U. The calculation is based on the investigation of the energy exchange between ship and incident wave, cf. 4. Following the thoughts of Liu and Papanikolaou (2020): (1) For $Fn = 0$, the added resistance and thus a_1 are negative, (2) on the green curve ($U = V_c/4$) it is assumed that the radiation component vanishes ($a_1 = 0$) and (3) on the orange curve ($U = V_c/2$) it is thought that C_{AW} is equal to the magnitude as in the head wave case, but for non-forward speed, i.e. a_1 is positive, but calculated for $Fn = 0$. In addition, (4) the value at any condition in between will be obtained by linear interpolation and (5) conditions above the orange curve will be approximated using the relative Froude number $Fn_r = \frac{U-V_c/2}{\sqrt{gL_{pp}}}$. The remaining regression coefficients are defined as follows:

$$a_2 = \begin{cases} 0.0072 + x_8 Fn & \text{for } Fn < 0.12 \\ Fn^{x_9} e^{(-x_{10} Fn)} & \text{for } Fn \geq 0.12 \end{cases} \tag{13}$$

$$a_3 = 1.0 + x_{11} \operatorname{atan} \frac{|T_a - T_f|}{L_{pp}} \tag{14}$$

$$b_1 = \begin{cases} x_{12} & \text{for } \bar{\omega} < 1 \\ -x_{13} & \text{elsewhere} \end{cases} \tag{15}$$

$$d_1 = \begin{cases} x_{14} \left(\frac{L_{pp} C_B}{B}\right)^{-x_{15}} & \text{for } \bar{\omega} < 1 \\ -x_{14} \left(\frac{L_{pp} C_B}{B}\right)^{-x_{15}} \times \left(4 - \frac{x_{16} \operatorname{atan}|T_a - T_f|}{L_{pp}}\right) & \text{elsewhere} \end{cases} \tag{16}$$

$$\bar{\omega} = x_{17} \sqrt[3]{k_{yy}} \sqrt{\frac{L_{pp}}{\lambda}} \left[1 - \frac{x_{18}}{C_B} \left(\ln \frac{B_m}{T_{max}} - \ln x_{19}\right)\right] \left(\frac{C_B}{x_{20}}\right)^{x_{21}} \times \left[\left(-x_{22}\, Fn^2 + x_{23}\, Fn\right) |\cos\beta| + \frac{x_{24}(13 + \cos 2\beta)}{x_{25}}\right]. \tag{17}$$

It is noted that T_{max} is defined as $T_{max} = \max(T_a, T_f)$. The remaining definitions are needed for the calculation of the reflection part, but are presented in the last part as modifications are introduced in these equations. Initially, the constraint enforcing the added resistance to be zero for $\lambda/L_{pp} > 2.5$ is removed in the draft coefficient α_{T*} as it led to discontinuous results after initial calibration attempts. Instead, the database was enriched with multiple artificial samples in the respective range of wavelengths with $C_{AW} = 0.0$ introducing domain knowledge into the otherwise solely data-driven methodology. Conversely, Cepowski (2020) did not include this kind of boundary condition in his empirical machine learning approach and in some cases the added resistance showed an unphysical increase in long waves. Referring to the initially defined uncertainty categories, the epistemic uncertainty in very long waves is reduced by the definition of artificial samples.

$$f(\beta) = \begin{cases} -\cos\beta & \text{for } \beta \in [\pi - E_1, 0] \\ 0 & \text{for } \beta < \pi - E_1 \end{cases} \tag{18}$$

$$\alpha_{T*} = 1 - e^{-x_{26}\pi \left(\frac{T^*}{\lambda} - \frac{T^*}{x_{27} L_{pp}}\right)}. \tag{19}$$

For the bow segments S_1 and S_2 the expression $T^* = T_{max}$ is valid. In the aft part, however, the following Eq. (20) is used. In the original paper, a condition was imposed at $C_B = 0.75$, but in the present approach, two separate parameter vectors are obtained with the transition at $C_B = 0.70$. Hence, the equation of T^* for the stern simplifies to:

$$T^* = \frac{T_{max} \left(x_{28} + \sqrt{|\cos\beta|}\right)}{x_{29}}. \tag{20}$$

The presented framework acts as a model in the following calibration or training procedure. Adopting the statistical notation, we consider the estimate of the semi-empirical framework C_{AW} as the approximation $\hat{y}_i$ and the database presented in Section 2 reflects the ground truth y_i. Ultimately, the presented formulation as well as the derived parameters are made publicly available on GitLab.[2]

3.2. Loss functions

As the performance of the semi-empirical method is not only subject to the uncertainty of the data, e.g. experimental uncertainty, but also to model form uncertainty, a parameter calibration approach is conducted. Essentially, we attempt to deduce an optimized parameter vector x_i using an objective or rather loss function and labeled data, i.e. the database. Generally speaking, this methodology is defined – in machine-learning terms – as Structural Risk Minimization (SRM) and its concrete form is defined in Eq. (21), cf. Wang et al. (2020).

$$\min \frac{1}{N} \sum_{i=1}^{N} \mathcal{L}_{x_i}(\hat{y}_i) \quad \text{where } \hat{y}_i = f(\theta_m) \tag{21}$$

In the above-mentioned equation, N corresponds to the number of samples and f denotes the previously presented semi-empirical formulation. The choice of the loss function $\mathcal{L}$ is highly influential on the quality of the results and is affected by the presence of outliers and noise in the data. For gradient-based optimization, e.g. stochastic gradient descent algorithms in deep learning, the differentiability of the loss function is of high importance. In this work, however, we use a gradient-free optimizer, i.e. particle swarm optimization. In Section 2 it was stated that the employed datasets are – the one for slender ships in particular – characterized by large variance and heteroskedasticity. For this reason, we investigate the effect of four different loss functions: (1) the squared loss, (2) the absolute loss, (3) the Huber loss and (4) the log-cosh loss. The latter two are, in fact, hybrid versions of the former two.

1. **Squared Loss**

   $$\mathcal{L}_{L2} = (y_i - \hat{y}_i)^2. \tag{22}$$

   The squared loss or $L2$ error is the most commonly used loss function and puts strong weight on outliers and variance.

2. **Absolute Loss**

   $$\mathcal{L}_{L1} = |y_i - \hat{y}_i|. \tag{23}$$

   The $L1$ or absolute error is robust and expresses the magnitude of errors without considering their direction.

Comparing the absolute to the squared loss, it proves that the $L2$ error is more stable and provides a closed form solution due to its continuous

[2] https://gitlab.gbar.dtu.dk/mamit/RAW_Formula.

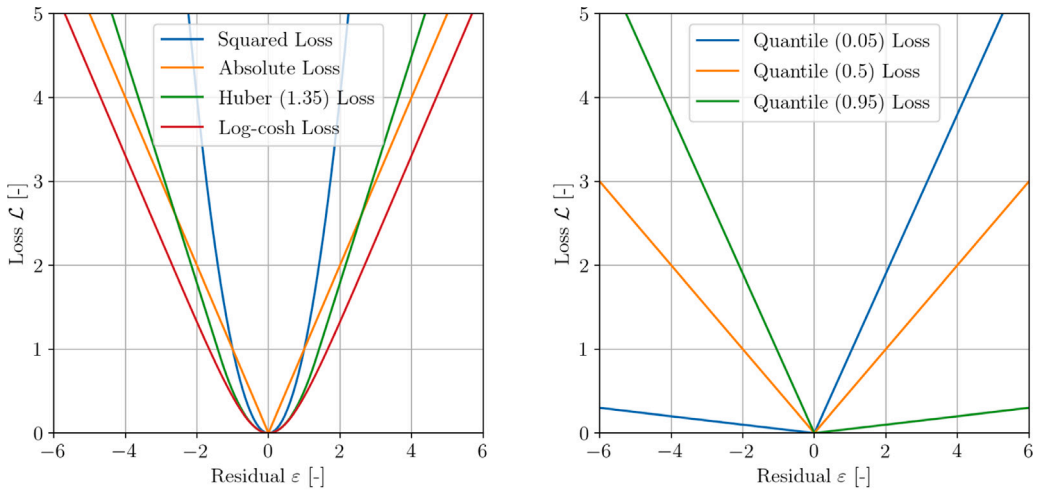

(a) Comparison of four different loss functions.

(b) Quantile loss functions for three different γ.

Fig. 5. Illustration of the behavior of the individual loss functions. (For interpretation of the references to color in this figure legend, the reader is referred to the web version of this article.)

derivative, Wang et al. (2020). Essentially, the Huber and the log-cosh losses are considered as elegant combinations of the $L1$ and $L2$ losses by restricting the influence of outliers and by also having a continuous derivative. Hence, they combine the advantages of both $L1$ and $L2$ loss.

3. **Huber Loss**

$$\mathcal{L}_{Huber} = \begin{cases} \frac{1}{2}(\hat{y}_i - y_i)^2 & \text{for } |\hat{y}_i - y_i| \leq \delta \\ \delta|\hat{y}_i - y_i| - \frac{1}{2}\delta^2 & \text{otherwise} \end{cases} \tag{24}$$

The Huber loss function is a piecewise function of squared and absolute loss. The transition is controlled by the hyperparameter δ and samples within this boundary use the squared loss, whereas outside the boundary it is vice versa. In doing so, the drawback of the squared loss can be diminished, i.e. putting less weight on outliers and thus avoiding overfitting. The use of the Huber loss is more complex due to the hyperparameter δ, but Huber himself suggested the robust value of $\delta = 1.35$, cf. Huber (1981).

4. **Log-cosh Loss**

$$\mathcal{L}_{log-cosh} = \log(\cosh(\hat{y}_i - y_i)). \tag{25}$$

The Log-cosh loss function is the logarithm of the hyperbolic cosine of the residual, i.e. when the error is small, the loss is close to $\frac{1}{2}\varepsilon^2$ and when the error is large, the loss is approximately $|\varepsilon| - \log 2$. Hence, its behavior is very similar to the Huber loss function, i.e. has all of its advantages, but it does not require the definition (and optimization) of a hyperparameter.

The individual loss functions are depicted in Fig. 5(a) and it is visible that the squared loss punishes large errors the most, whereas the absolute loss is the only discontinuous function. For more information about the described loss functions, cf. Wang et al. (2020).

The objective or loss function $\mathcal{L}$ of the parameter calibration is not subject to any equality or inequality constraints, but the search space Ω itself is constrained by lower and upper bounds of the variables $x_i^l \leq x_i \leq x_i^u, i = 1, \ldots, n$. The constraints of the design space are highly influential on the quality of the results and were found in an iterative process. Ultimately, the described methodology has a resemblance to a supervised regression approach in machine learning.

3.3. Quantile regression

Quantile Regression is a non-linear regression approach proposed by Koenker and Hallock (2001). Its application is considered herein as it is robust to the presence of outliers and considered as an extension to linear regression, i.e. in case the corresponding assumptions are not valid. This includes linearity, homoskedasticity and normality. As pointed out it Section 2, none of these prerequisites are met in the present work. Thus, for the determination of the uncertainty bounds, SRM is employed again (cf. Eq. (21)) and the quantile loss function is minimized. In general, this particular loss function is in its original form an extended version of the absolute loss, which qualitatively matches Eq. (23) when $\gamma = 0.5$ (i.e. the 50th percentile). The original quantile loss function as proposed by Koenker and Hallock (2001) is given in Eq. (26).

$$\mathcal{L}_\gamma(y, \hat{y}) = \begin{cases} (\gamma - 1)(y_i - \hat{y}_i) & \text{for } y_i < \hat{y}_i \\ \gamma(y_i - \hat{y}_i) & \text{otherwise} \end{cases} \quad \text{where the quantile is } \gamma \in [0, 1] \tag{26}$$

Using a tilted or *pinball* loss function in SRM enables the formula to reflect a specified quantile instead of the mean. Quantile loss functions adjust the weight of the individual sample's error according the given quantile γ, i.e. a smaller γ increases the magnitude of the loss of those samples with a negative residual ε and introduces more punishment for overestimation. For large γ it is vice versa. An illustration of several quantile loss functions are presented in Fig. 5(b) and for more elaborate details regarding quantile regression consult Koenker and Hallock (2001).

In this paper, a 90% prediction interval is desired and thus we choose two objective functions with $\gamma = 0.05$ and $\gamma = 0.95$. However, the actual definition of the used quantile loss function is dependent on the performance of the other four losses in the first stage, i.e. the parameter calibration. In addition, to the 29 parameters, an offset parameter x_{30} is defined and initialized with $x_{30} = \pm 0.1$, and is bounded by $x_{30} \in [0.0, 0.2]$. The updated and newly obtained parameters as well as the corresponding constraints will be presented in the following section.

4. Results and discussion

4.1. Parameter calibration

The following part presents the obtained results and their interpretation. It is noted that all samples of the S-Cb84 (cf. Table 1) are left out of the training dataset as it acts as an out-of-sample test case. Moreover, the training dataset comprises artificial samples in longer waves $\lambda/L_{pp} > 2.5$ as an enforced boundary condition. In Table 2,

Table 2
Initial, bounding and final values of the parameter vector. Note, that the values in the parentheses reflect the parameters of lower and upper bound, respectively.

	Baseline	Lower constraint	Upper constraint	Final parameters	
				$C_B < 0.70$	$C_B \geq 0.70$
x_1	4.0	3.0	8.0	4.06 {3.03,4.27}	6.99 {3.0,4.59}
x_2	0.5625	0.42	0.705	0.705 {0.42,0.705}	0.425 {0.420,0.565}
x_3	60.3	50	100	56.23 {49.97,55.88}	70.92 {55.84,54.28}
x_4	1.34	1	2	1.185 {1.66,1.06}	2.0 {1.329,1.236}
x_5	4.0	2.5	5	4.057 {3.466,5.0}	3.013 {4.312,5.0}
x_6	0.87	0.65	1.09	0.65 {1.09,0.65}	0.9 {1.09,0.65}
x_7	3.0	2.25	5	2.25 {3.53,2.538}	3.726 {3.75,2.25}
x_8	0.1676	0.1	0.3	0.134 {0.12,0.21}	0.281 {0.146,0.21}
x_9	1.5	1.2	1.9	1.626 {1.483,1.502}	1.388 {1.793,1.549}
x_{10}	3.5	2.5	4.5	3.585 {2.62,3.583}	3.869 {3.566,3.954}
x_{11}	28.7	22	36	29.107 {30.924,27.079}	17.963 {27.628,33.777}
x_{12}	11	8	14	10.868 {12.974,8.2}	11.5 {12.298,14.0}
x_{13}	8.5	5.5	10.7	9.878 {10.7,6.37}	5.589 {10.7,6.37}
x_{14}	566	425	800	480.961 {707.94,425.0}	473.743 {679.27,425.0}
x_{15}	2.66	1.95	3.5	2.62 {1.95,3.5}	2.214 {2.309,3.5}
x_{16}	125	100	200	123.163 {93.535,121.801}	153.646 {130.0,118.02}
x_{17}	2.142	1.6	5.0	1.745 {2.166,2.041}	2.433 {2.231,2.043}
x_{18}	0.111	0.08	0.3	0.107 {0.14,0.0836}	0.0557 {0.083,0.105}
x_{19}	2.75	1.0	3.5	3.5 {2.896,3.5}	2.410{2.638,2.268}
x_{20}	0.65	0.4	0.825	0.825 {0.825,0.639}	0.813 {0.784,0.702}
x_{21}	0.17	0.125	0.3	0.125 {0.131,0.125}	0.3 {0.22,0.125}
x_{22}	1.377	1.03	2.0	1.03 {1.03,1.03}	1.008 {1.351,1.03}
x_{23}	1.157	1.0	1.45	1.201 {1.422,1.134}	1.076 {1.318,1.45}
x_{24}	0.618	0.4	0.9	0.723 {0.632,0.603}	0.778 {0.627,0.647}
x_{25}	14.0	10	20	13.630 {17.286,12.364}	19.241 {15.26,14.423}
x_{26}	4	3.0	5.0	5.0 {3.0,5.0}	3.029 {3.0,3.0}
x_{27}	2.5	1.0	4.0	3.15 {3.114,3.15}	3.845 {2.408,3.15}
x_{28}	{4.0,2.0}	1.0	6.0	2.897 {6.0,1.0}	3.123 {6.0,1.0}
x_{29}	{5.0,3.0}	2.0	7.5	5.552 {2.0,7.5}	4.527 {2.0,7.5}
x_{30}	±0.1	0.0	±0.2	±0.2	±0.2

the derived parameters as well as the corresponding initial values and constraints are presented.

The determination of sensible constraints is the most time-consuming part, as their values affect the balance between over- and under-fitting, i.e. the *bias–variance-tradeoff*, cf. Hastie et al. (2009) for detailed information. Essentially, the presented parameter bounds were obtained in an iterative manner and the final values are, in fact, considered as relatively narrow. This is a result of the fact that the lower bound does not capture the resonance region sufficiently with broader constraints. Other than that, it seems that the constraints are chosen well since only a few final parameters reach the lower or upper bound. Moreover, noticeable differences between initial values and final parameters are observable underlining the degree of reduced uncertainty. Also the parameter vectors for $C_B \geq 0.70$ and $C_B < 0.70$ – both of mean and the bounds – differ notably in their magnitudes.

In this contribution, we consider the coefficient of determination R^2, the *Pearson* correlation coefficient r and the variance σ^2 as metrics for the assessment of the prediction accuracy. It is noted that the corresponding equations are presented in Eqs. (27)–(29) and that overbar indicates then mean.

$$R^2 = 1 - \frac{\Sigma(y_i - \hat{y}_i)^2}{\Sigma(y_i - \bar{y}_i)^2} \tag{27}$$

$$r = \frac{\Sigma(y_i - \bar{y})\Sigma(\hat{y}_i - \bar{\hat{y}}_i)}{\sqrt{\Sigma(y_i - \bar{y})^2 \Sigma(\hat{y}_i - \bar{\hat{y}})^2}} \tag{28}$$

$$\sigma^2 = \frac{1}{N}\sum_{i=1}^{N}(y_i - \hat{y}_i)^2. \tag{29}$$

The performance of the individual loss functions is examined for the whole database (cf. Section 2) and not the separate sets. It is noted that the database corresponds to the initial one and not to the training set. The metrics are presented in Table 3 and the results of the squared loss are highlighted as the derived parameters are most accurate and subsequently adopted.

Table 3
Metrics for the performance of individual parameter combinations on the whole database.

	Baseline	Squared loss	Absolute loss	Huber(1.35) loss	Log-cosh loss
R^2	0.672	**0.731**	0.711	0.722	0.721
r	0.835	**0.856**	0.848	0.852	0.852
σ^2	2.540	**2.074**	2.174	2.121	2.124

As can be inferred in Table 3, a performance increase of approximately 8.8% considering R^2 is achieved by the proposed methodology using parameters of the $L2$ procedure and compared to the metrics of the initial formulation. Moreover, the Pearson correlation coefficient improved and the variance decreased significantly across the board. The $L2$ loss performs superior compared to the $L1$ loss and the metrics of Huber and Log-cosh losses are of similar character as expected due to their comparable behavior. Lastly, the Breusch Pagan test is conducted for the residuals of the updated formula, but they are still heteroskedastic, since we have to reject H_0 again as the p-value is $p \ll 0.05$. The heteroskedasticity is also visible in the residuals plot in Fig. 6(a), in which the residuals of the original and updated formulation are displayed in parallel.

In general, the distinction between epistemic and aleatoric uncertainty is imprecise in the context of model assessment, Soize (2017). Hence, we introduce the term model form uncertainty dividing into *parameter* and *structural* uncertainty, where the latter corresponds to the model's bias, e.g. inadequate assumptions. The parameter calibration leads to a decrease in variance of the residuals, but, as indicated by the Breusch Pagan p-test, to no reduction in heteroskedasticity, cf. Fig. 6. Moreover, for low to medium magnitudes of the added resistance coefficient it is perceptible that the method tends to provide higher values compared to the database (overprediction). Whereas in the regime of large C_{AW} magnitude, the approach is characterized by underprediction, cf. Fig. 6(a). This shows strongly biased residuals and

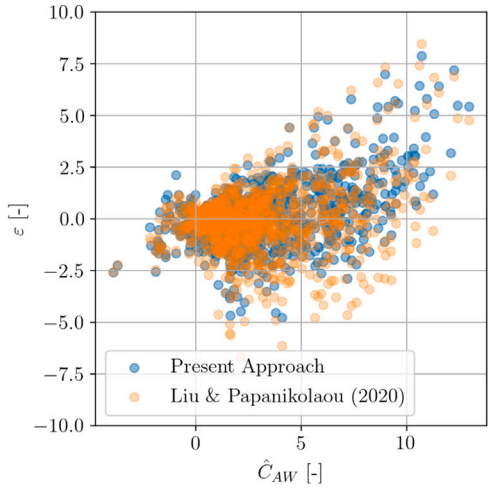

(a) Residuals ε presented for the added resistance coefficient C_{AW}.

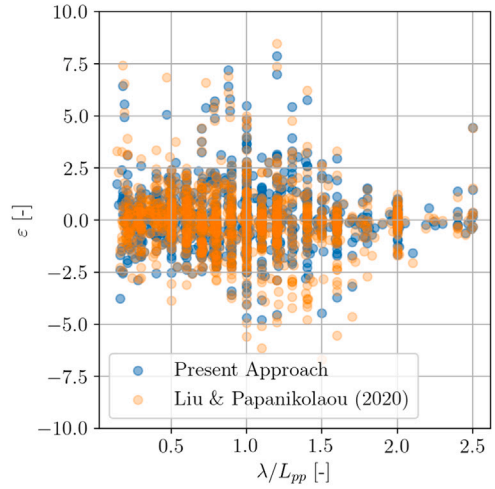

(b) Residuals ε presented for the relative wavelength λ/L_{pp}.

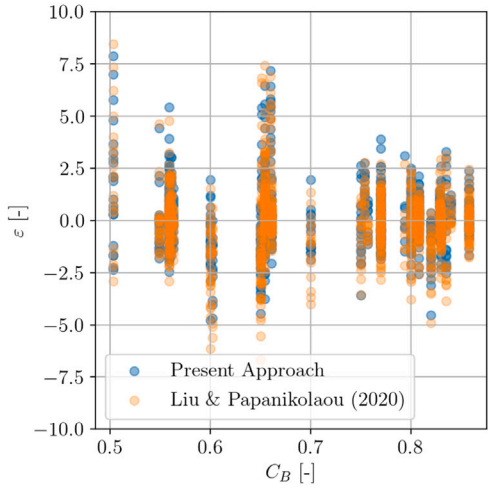

(c) Residuals ε presented for the block coefficient C_B.

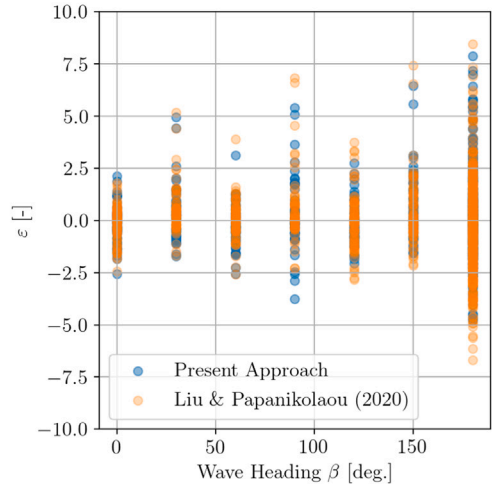

(d) Residuals ε presented for the wave heading β.

Fig. 6. Residual analysis comparing the presented approach to the original method. It is noted that the residuals are defined as $\epsilon_i = y_i - \hat{y}_i$, where y_i is considered as the ground truth. (For interpretation of the references to color in this figure legend, the reader is referred to the web version of this article.)

therefore considerable structural uncertainty. In view of Fig. 6(b) it is concluded that the largest residual variance is present in short waves and in the region close to resonant conditions (i.e. $\lambda/L_{pp} \in [0.5, 1.5]$). Ultimately, only a minor variance decrease is noticeable considering the blockcoefficient C_B and the wave heading β, cf. Figs. 6(c) and 6(d). However, the residuals are still biased towards lower estimates for slender hull shapes and also in head oblique wave conditions (i.e. $\beta \in [180, 150]$ deg.) Moreover, we see heavily skewed residuals for $\beta = 30$ deg. and a shift in the bias from the original to the present method in beam waves ($\beta = 90$ deg.). Ultimately, a substantial variance reduction (parameter uncertainty) was achieved, but the bias (structural uncertainty) remained stable to a large extend.

Since the parameters derived by minimizing the $L2$ loss are adopted, the squared version of the quantile loss function is used in the second task: The outlier robust quantile regression. The modified quantile loss function is defined in Eq. (30).

$$\mathcal{L}_{\gamma,L2}(y,\hat{y}) = \begin{cases} (\gamma-1)(y_i-\hat{y}_i)^2 & \text{for } y_i < \hat{y}_i \\ \gamma(y_i-\hat{y}_i)^2 & \text{otherwise.} \end{cases} \tag{30}$$

The convergence behavior of the determination of the four necessary uncertainty bounds is presented in Fig. 7, and it is stated that obtaining suitable parameters for the 90% prediction interval required more iterations, i.e. more computational effort, for the slender-type ships. Moreover, the corresponding values for the blunt-type ships are not only characterized by fewer iterations, but also by lower magnitude of the respective loss functions. This is a result of the sensitivity to large variance (outliers) of squared loss functions and the larger inherent variance in the case of the slender-type ship database. Ultimately, all four optimization runs converged successfully and the resulting parameters are presented in Table 2 in the parentheses.

4.2. Validation in regular waves

In the following, the validation of the developed method against model test results and other established (semi-)empirical methods for the determination of the added resistance is carried out. In this respect, we investigate four ships and illuminate the influence of forward-speed on the uncertainty, the in- and out-of-sample prediction in various wave headings as well as the comparison to established methods, e.g. the DTU design tool. It is noted that the corresponding main particulars of the individual test cases are listed in Table 1.

As in the original paper we validate the proposed method considering the S-Cb84 bulk carrier as an out-of-sample test case for the assessment of the overall generalization capability. The case ship is

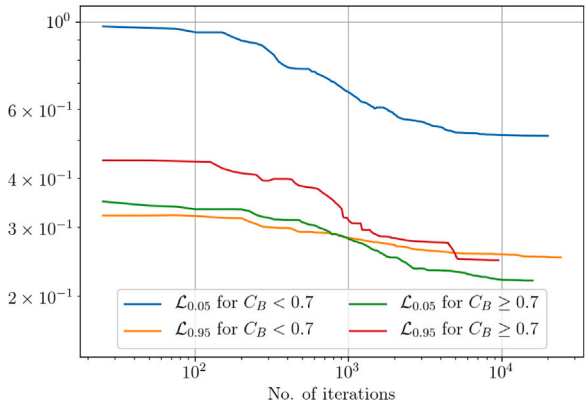

Fig. 7. Convergence study of the quantile loss functions for the individual bounds. Note that both axes are in logarithmic scale. (For interpretation of the references to color in this figure legend, the reader is referred to the web version of this article.)

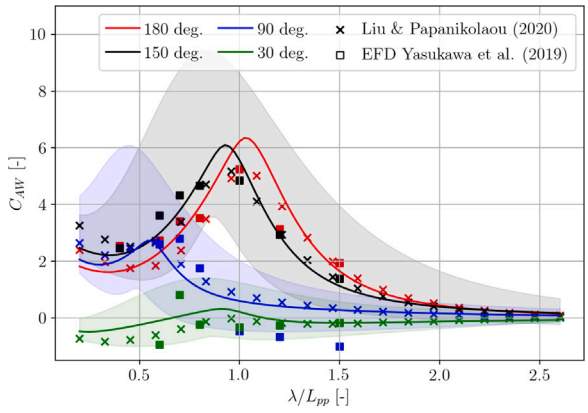

Fig. 8. Assessment of the performance for the out-of-sample test case S-Cb84 at $Fn = 0.1$. The uncertainty estimate for the head wave case is excluded, as it almost maps on top of the one for 150 deg. (For interpretation of the references to color in this figure legend, the reader is referred to the web version of this article.)

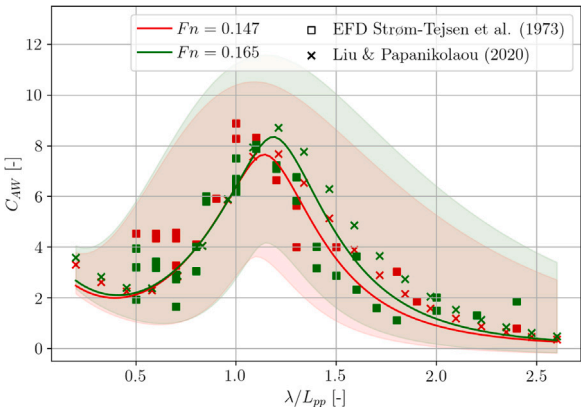

Fig. 9. Effect of forward speed investigating the S60 ship ($C_B = 0.8$) in head waves. (For interpretation of the references to color in this figure legend, the reader is referred to the web version of this article.)

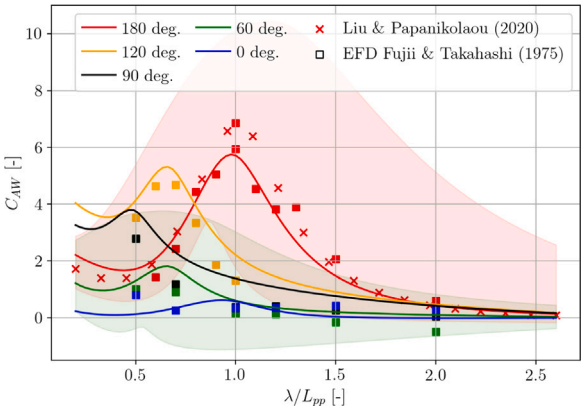

Fig. 10. S175 container ship at $Fn = 0.15$ for a variety of wave headings. As a sidenote, all experimental samples are taken from Fujii and Takahashi (1975). (For interpretation of the references to color in this figure legend, the reader is referred to the web version of this article.)

evaluated in several heading angles at $Fn = 0.1$ and the model test data is taken from Yasukawa et al. (2019).

As can be inferred from Fig. 8, the accuracy of the proposed method appears as sufficient in comparison to the original method. Moreover, the prediction interval is remarkably accurate and insightful, since almost all EFD (Experimental Fluid Dynamics) samples stay within the uncertainty bounds and the interval's width has a distinct dependency on the relative wavelength. The largest uncertainty is present in resonant conditions and the width narrows for short and especially for long waves. It is noted that the uncertainty estimate for head waves is not included as it intersects with the corresponding one of $\beta = 150$ deg. to a large extent. Even though the S-Cb84 was not part of the training dataset, the mean predictions are of comparable quality to the original method of Liu and Papanikolaou (2020).

The second case study is the Series 60 ship ($C_B = 0.8$) and the behavior of the uncertainty estimate in head waves with increasing forward speed is studied. The proposed method is validated against the EFD data from Strøm-Tejsen et al. (1973) in Fig. 9.

In view of Fig. 9, it is stated that all model test results remain inside the 90% prediction interval and also that the dependency of the uncertainty on the advance speed is evident. It is appreciated that the mean estimates of the proposed method provide lower predictions for the entire relative wavelength regime. Moreover, the peak frequency according to the semi-empirical formula deviates minimally from the experimental resonance frequency. Lastly, the variance increase with larger advance speed is not only visible for the 90% prediction intervals, but also in the EFD data itself.

The slender S175 container ship is the third test case and will be examined for five different heading angles in Fig. 10 at $Fn = 0.15$. The experimental results of Fujii and Takahashi (1975) are considered in the following.

All of the EFD samples stay well within the uncertainty bounds and the present method's mean predictions show sufficient agreement to the model test results in all considered heading angles, but tend to underestimate the non-dimensional added resistance in long head waves. In addition, it evident that the proposed approach provides higher mean estimates in short waves, but lower ones in resonant conditions compared to the original method. This is the exact opposite to the observations made for the S-Cb84 bulk carrier. The final case study is a full-type LNG carrier in oblique waves with $\beta = 150$ deg. and moderate forward speed at $Fn = 0.19$. The proposed method will be compared to several well-established approaches, such as the STAwaveII (ITTC, 2017), the DTU design tool, the CTH formula proposed by Lang and Mao (2021) and the original approach by Liu and Papanikolaou (2020). All of these formulations were introduced in Section 1.1. The model test results of Kim et al. (2021) are considered as the ground truth in Fig. 11.

As one can appreciate in Fig. 11, the uncertainty bounds enclose the majority of the EFD results. Moreover, the mean estimate of the present

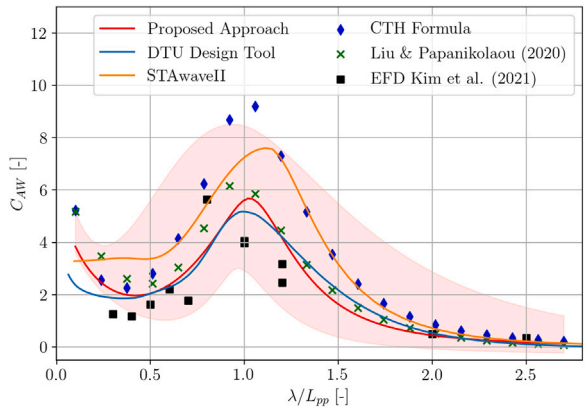

Fig. 11. Comparison of several prediction methods for the S-LNGC at $Fn = 0.19$ in $\beta = 150$ deg. (For interpretation of the references to color in this figure legend, the reader is referred to the web version of this article.)

method tends towards the lower bound in very short waves, which might indicate that the parameter constraints in the above methodology were selected too narrow as two samples fall outside the prediction interval in the short wave regime. Other than that, the present method approximates the non-dimensional added resistance well and is in satisfactory agreement with the DTU design tool. The STAwaveII and the CTH formula show the tendency to over predict the added resistance in the resonance region as well as for long waves and the estimates of the CTH formula even fall outside the 90% prediction interval. It is assumed that the deviation in case of the CTH formula estimates results from the two opposing approaches for the calculation of the reflection contribution as both the CTH and Liu and Papanikolaou (2020) formulas apply the (Jinkine and Ferdinande, 1974) approach for the motion component. Furthermore, Lang and Mao (2021) derive a different, simplified methodology for the calculation of added resistance in oblique and following seas from the analysis of heave, pitch and roll transfer functions and introduce two additional correction coefficients. Comparing the original formula of Liu and Papanikolaou (2020) to the calibrated one, we conclude that the same observations as in the case of the S60 ship are perceptible, i.e. lower estimates for the whole range of relative wavelengths. Lastly, it is not possible to properly assess the performance in very short waves (i.e. $\lambda/L_{pp} < 0.3$) as there are no available model test results.

4.3. General remarks and discussion

The mean estimate of the proposed method is of comparable accuracy to the original formula; however, the prediction interval proved to be highly insightful and shows that the reliable and accurate estimation of the second order wave drift force on ships is still a complex research area. The *quantitative* prediction of uncertainty around the added resistance is the main novelty of this contribution. In general, the shape of the 90% prediction interval matches expectations to a large extend, but especially in very short waves the uncertainties were assumed to be larger. In case of the S-LNGC this fact was most striking as the mean estimate converged towards the lower uncertainty bound and the EFD data fell out of the prediction interval, cf. Fig. 11. The narrow bandwidth in the short wave regime results from the epistemic uncertainty and the limited availability of samples in this range of relative wavelengths, cf. Fig. 1(b).

Moreover, one can conclude in view of Fig. 10, that the reflection component $C_{AW,R}$ has increased for slender ships relative to the formula of Liu and Papanikolaou (2020), whereas for the motion contribution $C_{AW,M}$ it is vice versa. For blunt-type ships, it is visible that the reflection component has decreased considerably, cf. Fig. 9. In Section 2, it was assumed that the large variance in the slender ship ($C_B < 0.7$) database is attributed to high forward speeds. Additionally, the variance might result from more pronounced non-linear behavior, such as wave breaking in short waves, which is mainly due to the hull shape (and wave steepness): (1) The significant flare angles in the bow region, (2) the relatively long bulbous bow and (3) extreme B/T ratios (in case of passenger ships) lead to a considerable reflection contribution. Hizir et al. (2019) discuss the *geometric non-linearity* of slender hulls and Mourkogiannis and Liu (2021) analyze the bow reflection of ships with high B/T ratios both analytically and numerically. The accuracy for blunt and slender ships as well as the smoothness of the method is investigated in Fig. 12 considering the HSVA cruise ship and the SNU tanker. It is noted that both ships are in-sample testcases and that the proper assessment and validation of the formula's accuracy is not possible using a tilted three-dimensional figure.

It is thought that the presented method provides satisfactory and smooth estimates, but fine-tuning is needed especially in short waves as considerable deviations are evident in both Figs. 12(a) and 12(b). Moreover, conservative estimates for the full-type tanker and underprediction for the fast and slender cruise ship are perceptible. The latter problem has already been observed in Fig. 2 and similar deviations for slender ships were also observed by Tsujimoto et al. (2008) using their NMRI formula. Lastly, the reduction of the residuals' variance was achieved and thus it was possible to diminish the parameter uncertainty. However, even after the parameter calibration, the residuals revealed significant bias in Fig. 6 indicating strong structural uncertainty. Although it was attempted to lower this uncertainty component by splitting the method at $C_B = 0.70$ and deriving two separate parameter sets, the impact was negligible. The extension of the underlying semi-empirical framework of Liu and Papanikolaou (2020) is thus an important aspect for the reduction of structural uncertainty. As a sidenote, during extensive validation studies it appeared in a few cases that in following seas and relatively low forward speed ($Fn < 0.1$) the uncertainty bounds intersect. It is thought that this results from the small magnitude of the added resistance for low Fn and the conditional calculation of a_1. Ultimately, an exception is included in the developed code to circumvent this drawback and it also requires further studies in the future in order to overcome this issue.

The calculation of the added resistance in following and quartering waves utilizing the Liu and Papanikolaou formula is based on linear interpolation and dependent on encounter frequency. The formulation of Maruo (1957), on the other hand, is exact under the assumptions of an ideal fluid and shows that the sign of the added resistance in following waves can be obtained by the balance of the magnitude of three integrals dependent on the encounter frequency. Still, the drawback of this approach is the required knowledge of detailed hull form information as well as the increased computational effort for the calculation of the Kochin function. However, the focus of the presented formula is on the efficient and practical determination of the added resistance in waves with rudimentary hull form information, e.g. in early ship design stages. Therefore, a modified and simplified reasoning using Maruo's theory is chosen for the calculation of the sign of the added resistance in following waves (cf. Eq. (12) and Fig. 4). In addition, the development of a correction approach dependent on wave steepness would lead to improved results of the semi-empirical framework especially in short waves and for slender ships, however, there is often a lack of corresponding H/λ data in publicly available experimental data.

The previously mentioned assumption of the DTU design tool and the NMRI formula, i.e. considering the added resistance to be zero in stern oblique waves due to the surrounding uncertainty is addressed. From a practical perspective the assumption appears as legitimate in view of Figs. 8 and 10 as the degree of uncertainty engulfs the actual magnitude of the predicted added resistance. However, from a scientific standpoint this observation motivates further rigorous experimental

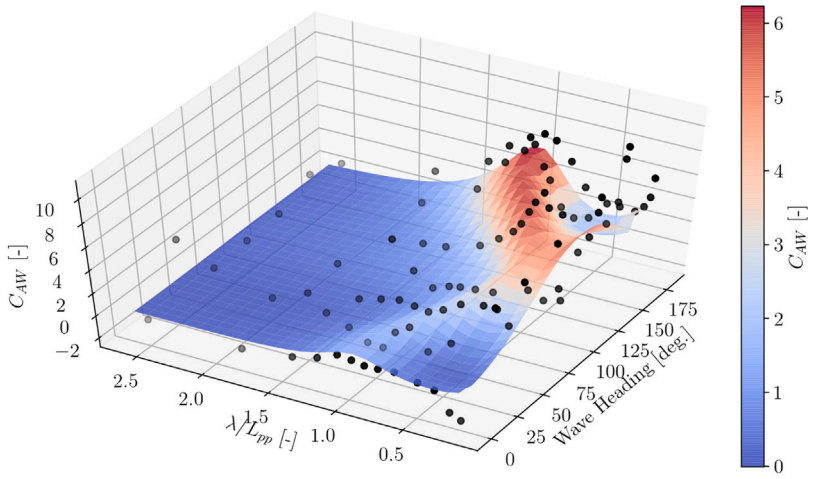

(a) Slender HSVA cruise ship ($Fn = 0.233$), cf. Valanto and Hong (2015).

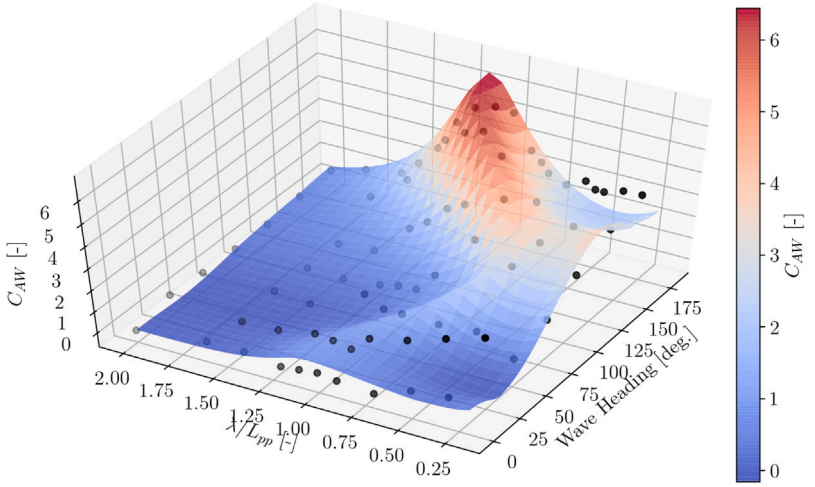

(b) Full-type SNU tanker ($Fn = 0.137$), cf. Park et al. (2019).

Fig. 12. Illustration of the present method compared to model test data for two case studies. (For interpretation of the references to color in this figure legend, the reader is referred to the web version of this article.)

and numerical investigation of C_{AW} in wave headings of $\beta \in [0, 90]$ deg., in order to further reduce the epistemic uncertainty in this regime of wave headings. In addition, more experimental data for slender ships, e.g. container and naval ships, are required. It is well known in statistical modeling that the model itself can only be as good as the underlying dataset. Hence, the extension of the database with model test samples showing high data quality in oblique waves is essential for the enhancement of the Liu and Papanikolaou formula applying the present approach.

The prediction of uncertainty bounds of the added resistance enables the possible application of the proposed method for the determination of outliers and erroneous data, i.e. *outlier detection*, in either experimental or numerical data. The definition of a corresponding decision boundary is non-trivial in this case as the added resistance is inherently non-linear (and heteroskedastic). Hence, a constant (i.e. linear) criterion for anomaly detection for the entire C_{AW} regime derived, e.g. from either the variance or the interquartile range of the underlying dataset is considered as not appropriate. In this respect, the application of unsupervised machine learning methods for classification show potential for accurate non-linear outlier detection for C_{AW}. However, this kind of methods is in general considered as opaque and thus the proposed approach could show better applicability due to its transparency resulting from the used simple algebraic expressions. Ultimately, an investigation in this direction is an interesting aspect for further work.

5. Summary and conclusion

The present study proposed a data-driven methodology for parameter calibration of a semi-empirical approach for estimation of the added resistance. The calibration was performed for the reduction of the inherent uncertainties of the added resistance in a deterministic manner. In this contribution, the mathematical formulation of Liu and Papanikolaou (2020) was adjusted and the parameter vector was optimized with respect to two datasets for full and slender ships consisting of several hundred of data points from publicly available model tests resembling the current world fleet sufficiently. In doing so, the method's transparency is maintained and the advantages of supervised regression models are leveraged. The minimization was defined as a single objective optimization problem and due to the complex and scattered loss landscape, the stochastic and metaheuristic particle swarm optimizer was used. It was found that out of four different loss functions, the squared loss function performed superior according to the chosen metrics. The calibration of the semi-empirical definition led to an increase of around 9% in performance and thereby the parameter uncertainty was diminished significantly. The 90% prediction interval was established by deriving additional parameter sets which were

determined by optimizing the tilted quantile version of the squared loss function. The uncertainty bounds proved to be highly valuable in a practical context for expressing the inherent irreducible uncertainty of the added resistance. Finally, the proposed method was validated against experimental data and several well-established formulas for the prediction of the added resistance. The validation studies suggest satisfactory accuracy of the mean estimate and the prediction interval on in- and out-of-sample data.

The implementation of the uncertainty bounds increases the relevance of the used formula for practical application. In addition, the described calibration methodology is considered as "method-agnostic" or generic for uncertainty quantification of (semi-)empirical formulas in general for e.g. the calculation of motion transfer functions using the closed form expressions of Jensen et al. (2004) as long as enough experimental data is available. The present study was limited to regular long-crested regular waves, however, the calculation of the mean added resistance in irregular waves is trivial given a suitable (directional) wave energy density spectrum and under the assumption of linear superposition and time invariance. However, the mentioned prerequisites are invalid under certain circumstances, e.g. in severe sea states or under changing weather conditions. For this reason, higher order spectral analysis may be required for an accurate estimate of the mean added resistance in a realistic seaway as shown by Hasselmann (1966). Furthermore, a corresponding uncertainty estimate of the prevalent wave spectrum is necessary for a consistent calculation. Lastly, the present paper advocates the implementation of a trustworthy representation of uncertainty when predicting safety-related quantities in ship hydrodynamics, such as the added resistance or speed loss in a realistic seaway.

Even though the method has been compared to multiple established approaches, additional and more rigorous validation studies are necessary for universal applicable recommendations and limitations for application. Moreover, sensitivity studies for the variation in draft and trim are important subjects of future work, in order to prove the applicability of the proposed method in ship operation for, e.g. performance monitoring or weather routing. Moreover, it seems appealing to enrich the presented database with high-fidelity CFD results – in short and oblique waves in particular – for further reduction of epistemic uncertainty as model test results from the public domain are scarce in these specific conditions. In Section 2, it was decided to split the approach for the block coefficient; however, dividing the method for different forward speed regimes and deriving updated parameter sets might have serious potential for further reducing structural uncertainty. The application of a parameter calibration combined with a bias correction introduced by an additive discrepancy expression in a probabilistic or Bayesian methodology could also have a tremendous effect on reducing and *explaining* the model form uncertainty, cf. Wu et al. (2021).

Reproducibility

In order to facilitate adoption and adaptation of the presented approach, the Python code as well as an Excel implementation is publicly available on https://gitlab.gbar.dtu.dk/mamit/RAW_Formula.

CRediT authorship contribution statement

Malte Mittendorf: Conceptualization, Methodology, Software, Formal analysis, Investigation, Data curation, Validation, Visualization, Writing – original draft, Writing – review & editing. **Ulrik D. Nielsen:** Writing – review & editing, Supervision, Project administration, Resources, Funding acquisition. **Harry B. Bingham:** Writing – review & editing, Supervision, Resources, Project administration. **Shukui Liu:** Writing – review & editing, Software, Resources.

Declaration of competing interest

The authors declare that they have no known competing financial interests or personal relationships that could have appeared to influence the work reported in this paper.

Acknowledgments

The authors express their gratitude towards Professor Papanikolaou (NTUA) for general discussions and guiding suggestions. In addition, the valuable feedback by a number of anonymous reviewers is greatly acknowledged. The financial support from The Danish Maritime Fund (Projekt 2019-043), A/S D/S Orient's Fond and the Department of Mechanical Engineering (DTU) is highly appreciated. The second author received funding by the Research Council of Norway through the Centres of Excellence scheme, project number 223254 AMOS. All authors approved the version of the manuscript to be published.

References

Amini-Afshar, M., Bingham, H.B., 2021. Added resistance using salvesen – tuck – faltinsen strip theory and the kochin function. Appl. Ocean Res. 106, 102481.
Blank, J., Deb, K., 2020. Pymoo: Multi-objective optimization in python. IEEE Access 8, 89497–89509.
Blok, J.J., 1993. The Resistance Increase of a Ship in Waves (Ph.D. thesis). Technical University of Delft.
Bolbot, V., Papanikolaou, A., 2016. Parametric, multi-objective optimisation of ships bow for the added resistance in waves. Ship Technol. Res. 63 (3), 171–180.
Breusch, T.S., Pagan, A.R., 1979. A simple test for heteroskedasticity and random coefficient variation. Econometrica 47 (5), 1287–1294.
Cepowski, T., 2020. The prediction of ship added resistance at the preliminary design stage by the use of an artificial neural network. J. Ocean Eng. 195.
Equasis, 2019. Statistics from Equasis - Electronic Quality Ship Information System. The 2019 World Fleet Report.
Faltinsen, O.M., Minsaas, K.J., Liapis, N., Skjordal, S.O., 1980. Prediction of resistance and propulsion of a ship in a seaway. In: Proc. of 13th Symposium on Naval Hydrodynamics. Tokyo (Japan): The Shipbuilding Research Association of Japan. pp. 505–529.
Fujii, H., Takahashi, T., 1975. Experimental study on the resistance increase of a large full ship in regular oblique waves. J. Soc. Nav. Archit. Japan 137, 132–137.
Gatchell, S., 2018. Stability and Hydrodynamic Tools – Level 1. HOLISHIP Internal Report D3.2.
Gerritsma, J., Beukelman, W., 1972. Analysis of the resistance increase in waves of a fast cargo-ship. Int. Shipbuild. Prog. 18 (217).
Guo, B., Steen, S., 2010. Added resistance of a VLCC in short waves. In: Proc. 29th Int. Conf. on Ocean, Offshore & Arctic Engineering. OMAE 2010.
Hasselmann, K., 1966. On non-linear ship motions in irregular waves. J. Ship Res. 10, 64–68.
Hastie, T., Tibshirani, R., Friedman, J., 2009. Elements of Statistical Learning: Data Mining, Inference, and Prediction, second ed. Springer Science+Business Media, New York.
Havelock, T.H., 1940. The pressure of water waves upon a fixed obstacle. Proc. R. Soc. Lond. Ser. A 175 (963), 409–421.
Hizir, O., Kim, M., Turan, O., Day, A., Incecik, A., Lee, Y., 2019. Numerical studies on non-linearity of added resistance and ship motions of KVLCC2 in short and long waves. Int. J. Nav. Archit. Ocean Eng. 11 (1), 143–153.
Hollenbach, K.U., 1998. Estimating resistance and propulsion for single-screw and twin-screw ships. J. Ship Tech. Res. 45 (2), 72–76.
Holt, P., Nielsen, U.D., 2021. Preliminary assessment of increased main engine load as a consequence of added wave resistance in the light of minimum propulsion power. J. Appl. Ocean Res. 108, 102543.
Holtrop, J., Mennen, G., 1982. An approximate power prediction method. Int. Shipbuild. Prog. 29 (335), 166–170.
Huber, P.J., 1981. Robust Statistics. John Wiley and Sons, New York.
Hüllermeier, E., Waegeman, W., 2021. Aleatoric and epistemic uncertainty in machine learning: an introduction to concepts and methods. Mach. Learn. 110, 457–506.
IMO, 2013. Interim guidelines for determining minimum propulsion power to maintain the maneuverability in adverse conditions. London, international maritime organization. In: MEPC 232(65), London, UK.
IMO, 2016. Supplementary information on the draft revised guidelines for determining minimum propulsion power to maintain the maneuverability of ships in adverse conditions. In: MEPC 70/INF.30, London, UK.
IMO, 2017. Draft revised guidelines for determining minimum propulsion power to maintain the manoeuvrability of ships in adverse conditions. In: MEPC 71/INF.28. London, UK.

IMO, 2021. Report of the correspondence group on air pollution and energy efficiency, submitted by Japan. In: MEPC 76/5/1, London, UK.
ITTC, 2014. Procedures and guidelines: Prediction of power increase in irregular waves from model test. In: International Towing Tank Conference.
ITTC, 2017. Recommended procedures and guidelines - preparation, conduct and analysis of speed/power trials. In: International Towing Tank Conference.
ITTC, 2021. The specialist committee on ships in operation at sea (SOS): Final report and recommendations to the 29th ITTC. In: International Towing Tank Conference.
Jensen, J.J., Mansour, A.E., Olsen, A.S., 2004. Estimation of ship motions using closed-form expressions. Ocean Eng. 31 (1), 61–85.
Jinkine, V., Ferdinande, V., 1974. A method for predicting the added resistance of fast cargo ships in head waves. Int. Shipbuild. Prog. 21 (238), 149–167.
Kadomatsu, K., Inoue, Y., Takarada, N., 1989. On the added resistance and speed loss in low forward speed range. J. Soc. Nav. Archit. Japan 166, 217–223.
Kashiwagi, M., 2013. Hydrodynamic study on added resistance using unsteady wave analysis. J. Ship Res. 57 (4), 220–240.
Kashiwagi, M., Ikeda, T., Sasakawa, T., 2010. Effects of forward speed of a ship on added resistance in waves. Int. J. Offshore Polar Eng. 20 (3), 196–203.
Kashiwagi, M., Iwashita, H., Miura, S., Hinatsu, M., 2019. Study on added resistance with measured unsteady pressure distribution on ship-hull surface. In: Proc. of 34th IWWWFB (Noah's on the Beach, Newcastle, NSW, Australia). pp. 81–84.
Kashiwagi, M., Sugimoto, K., Ueda, T., Yamasaki, K., Arihama, K., Kimura, K., Yamashita, R., Itoh, A., Mizokami, S., 2004. An analysis system for propulsive performance in waves. J. Kansai Soc. Nav. Archit. 241, 67–82.
Kennedy, J., Eberhart, R., 1995. Particle swarm optimization. In: Proc. of IEEE Int. Conf. on Neural Networks, Vol. IV. pp. 1942–1948.
Kim, T., Yoo, S., Kim, H.J., 2021. Estimation of added resistance of an LNG carrier in oblique waves. J. Ocean Eng. 231, 109068.
Koenker, R., Hallock, K.F., 2001. Quantile regression. J. Econ. Perspect. 15 (4), 143–156.
Kuroda, M., Tsujimoto, M., Fujiwara, T., 2008. Investigation on components of added resistance in short waves. J. Soc. Nav. Archit. Ocean Eng. 8.
Kwon, Y.J., 1981. The Effect of Weather, Particularly Short Sea Waves, on Ship Speed Performance (Ph.D. thesis). Department of Naval Architecture and Shipbuilding, University of Newcastle upon Tyne.
Lang, X., Mao, W., 2021. A practical speed loss prediction model at arbitrary wave heading for ship voyage optimization. J. Mar. Sci. Appl. 20, 410–425.
Li, C., Ma, X., Chen, W., Li, J., Dong, G., 2016. Experimental investigation of self propulsion factor for a ship in regular waves. J. Shipbuild. China 57 (1), 1–8.
Liu, S., 2020. Revisiting the influence of a ship's draft on the drift force due to diffraction effect. J. Ship Tech. Res. 67 (3), 175–180.
Liu, S., Papanikolaou, A., 2013. Added resistance of ships in quartering seas. In: Proc. V Int. Conf. on Computational Methods for Coupled Problems in Science and Engineering Coupled Problems 2013, Spain.
Liu, S., Papanikolaou, A., 2016. Fast approach to the estimation of the added resistance of ships in head waves. J. Ocean Eng. 112, 211–225.
Liu, S., Papanikolaou, A., 2020. Regression analysis of experimental data for added resistance in waves of arbitrary heading and development of a semi-empirical formula. J. Ocean Eng. 206.
Liu, S., Papanikolaou, A., Zaraphonitis, G., 2015. Practical approach to the added resistance of a ship in short waves. In: Proc. of the 25th Int. Offshore and Polar Engineering Conference, Kona, Hawaii, ISOPE.
Liu, S., Shang, B., Papanikolaou, A., 2019. On the resistance and speed loss of full type ships in a seaway. J. Ship Tech. Res. 66 (3), 161–179.
Martinsen, M.A., 2016. A Design Tool for Estimating Wave Added Resistance of Container Ships (Master's Thesis). Technical University of Denmark.
Maruo, H., 1957. The excess resistance of a ship in rough seas. Int. Shipbuild. Prog. 4 (35).
McKay, M.D., Beckman, R.J., Conover, W.J., 1979. A comparison of three methods for selecting values of input variables in the analysis of output from a computer code. Technometrics 21 (2), 239–245.
Mikkelsen, H., Shao, Y., Walther, J.H., 2022. Numerical study of nominal wake fields of a container ship in oblique regular waves. Appl. Ocean Res. 119, 102968.
Minsaas, K., Faltinsen, O.M., Persson, B., 1983. On the importance of added resistance, propeller immersion and propeller ventilation for large ships in a seaway. In: Proc. of 2nd Int. Symp. on Practical Design in Shipbuilding (PRADS'83), Tokyo and Seoul.
Mittendorf, M., Nielsen, U.D., Bingham, H.B., 2022. Data-driven prediction of added-wave resistance on ships in oblique waves - a comparison between tree-based ensemble methods and artificial neural networks. J. Appl. Ocean Res. 118 (102964).
Mourkogiannis, D., Liu, S., 2021. Investigation of the influence of the main dimensional ratios of a ship on the added resistance and drift force in short waves. In: Proc. of 31st Int. Ocean and Polar Engineering Conference, Rhodes, Greece (Virtual).
Nakamura, S., Naito, S., 1977. Propulsive performance of a containership in waves. J. Soc. Nav. Archit. Japan 15, 24–48.
Nielsen, C.S., 2015. A Ship Design Tool for Estimating Added Resistance in Waves (Master's Thesis). Technical University of Denmark.
Nikolopoulos, L., Boulougouris, E., 2019. A study on the statistical calibration of the holtrop and mennen approximate power prediction method for full hull form, low froude number vessels. J. Ship. Prod. Des. 35, 41–68.
Oh, S., Yang, J., Park, S.H., 2015. Computational and experimental studies on added resistance of aframax-class tankers in head seas. J. Soc. Nav. Archit. Korea 52 (6), 471–477.
Papanikolaou, A., 2014. Ship Design – Methodologies of Preliminary Design. Springer.
Papanikolaou, A.D., 2018. Hydrodynamics & ship design: Optimization of ships for minimum power and safe navigation in adverse weather conditions. In: 41st Georg Weinblum Memorial Lecture, Hamburg.
Papanikolaou, A., Liu, S., 2021. On the uncertainties in the estimation of the added resistance of ships in waves in view of practical applications. In: Proc. of 5th Joint ISSC and ITTC International Workshop on Uncertainty Modelling in Wave Description and Wave Induced Responses.
Park, D.M., Lee, J., Jung, Y., Lee, J., Kim, Y., Gerhardt, F., 2019. Experimental and numerical studies on added resistance of ship in oblique sea conditions. J. Ocean Eng. 186, 106070.
Park, D.M., Lee, J., Kim, Y., 2015. Uncertainty analysis for added resistance experiment of KVLCC2 ship. J. Ocean Eng. 95, 143–156.
Sadat-Hosseini, H., Wu, P., Carrica, P., Kim, H., Toda, Y., Stern, F., 2013. CFD verification and validation of added resistance and motions of KVLCC2 with fixed and free surge in short and long head waves. J. Ocean Eng. 59, 240–273.
Shigunov, V., el Moctar, O., Papanikolaou, A., Potthoff, R., Liu, S., 2018. International benchmark study on numerical simulation methods for prediction of maneuverability of ships in waves. J. Ocean Eng. 165, 365–385.
Sigmund, S., 2018. Performance of Ships in Waves (Ph.D. thesis). University of Duisburg-Essen.
Simonsen, C.D., Otzen, J.F., Nielsen, C., Stern, F., 2014. CFD prediction of added resistance of the KCS in regular head and oblique waves. In: Proc. of 30th Symp. on Naval Hydrodynamics, Hobart, Tasmania, Australia.
Söding, H., Shigunov, V., Schellin, T., el Moctar, O., 2014. A rankine panel method for added resistance of ships in waves. J. Offshore Mech. Arct. Eng. 136.
Soize, C., 2017. Uncertainty Quantification: An Accelerated Course with Advanced Applications in Computational Engineering. In: Interdisciplinary Applied Mathematics, vol. 47, Springer.
Sprenger, F., Maron, A., Delefortrie, G., Hochbaum, A., Fathi, D., 2015. Mid-term review of tank test results. In: SHOPERA Deliverable D3 2.
Sprenger, F., Maron, A., Delefortrie, G., Van Zwijnsvoorde, T., Cura-Hochbaum, A., Lengwinat, A., Papanikolaou, A., 2017. Experimental studies on seakeeping and manoeuvrability in adverse conditions.. J. Ship Res. 61 (3), 131–152.
SSPA, 2012. Ulysses project phase II: Seakeeping test for 2020 ship in sspa's maritime dynamic laboratory. In: ULYSSES Seakeeping and Manoeuvring Model Tests.
Stocker, M.R., 2016. Surge Free Added Resistance Tests in Oblique Wave Headings for the KRISO Container Ship Model (M.Sc. Thesis). University of Iowa.
Strøm-Tejsen, J., Yeh, H.Y.H., Moran, D.D., 1973. Added resistance in waves. Soc. Nav. Archit. Mar. Eng. Trans. 81, 109–143.
Takahashi, T., 1988. A practical prediction method of added resistance of a ship in waves and the direction of its application to hull form design. Trans. West Japan Soc. Nav. Archit. 75, 75–95.
Taskar, B., Andersen, P., 2021. Comparison of added resistance methods using digital twin and full-scale data. J. Ocean Eng. 229, 108710.
Tsujimoto, M., Shibata, K., Kuroda, M., Takagi, K., 2008. A practical correction method for added resistance in waves. J. Japan Soc. Nav. Archit. Ocean Eng. 8, 177–184.
Tsujimoto, M., Yasukawa, H., Yamamoto, K., Il Lee, T., 2021. Validation of added resistance in waves by tank tests and sea trial data. J. Ship Tech. Res..
Uharek, S., 2019. Numerical Prediction of Ship Manoeuvering Performance in Waves (Doctoral Thesis). Technical University of Berlin.
Ursell, F., Dean, W.R., 1947. The effect of a fixed vertical barrier on surface waves in deep water. Math. Proc. Cambridge Philos. Soc. 43 (3), 374–382.
Valanto, P., Hong, Y., 2015. Experimental investigation on ship wave added resistance in regular head, oblique, beam, and following waves. In: Proc. of the 25th Int. Society of Offshore and Polar Engineers.
Wang, J., Bielicki, S., Kluwe, F., Xin, G., Orihara, H., Kume, K., Oh, S., Liu, S., Feng, P., 2021. Validation study on a new semi-empirical method for the prediction of added resistance in waves of arbitrary heading in analyzing ship speed trial results. J. Ocean Eng. 240, 109959.
Wang, Q., Ma, Y., Zhao, K., Tian, Y., 2020. A comprehensive survey of loss functions in machine learning. Ann. Data Sci..
Wu, X., Xie, Z., Alsafadi, F., Kozlowski, T., 2021. A comprehensive survey of inverse uncertainty quantification of physical model parameters in nuclear system thermal-hydraulics codes. arXiv:2104.12919v1.
Yang, K., Kim, Y., Jung, Y., 2018. Enhancement of asymptotic formula for added resistance of ships in short waves. J. Ocean Eng. 148, 211–222.
Yasukawa, H., Hirata, N., Matsumoto, A., Kuroiwa, R., Mizokami, S., 2019. Evaluations of wave-induced steady forces and turning motion of a full hull ship in waves. J. Mar. Sci. Technol. 24 (1), 1–15.
Yasukawa, H., Tsujimoto, M., 2020. Impact of bow shape on added resistance of a full hull ship in head waves. J. Ship Tech. Res. 67 (3), 136–147.
Yu, J.W., Lee, C.M., Lee, I., Choi, J.E., 2017. Bow hull-form optimization in waves of a 66,000 DWT bulk carrier. Int. J. Naval. Archit. Ocean. Eng. 9 (5), 499–508.
Zhan, Z., Zhang, J., Li, Y., Chung, H.S., 2009. Adaptive particle swarm optimization. IEEE Trans. Syst. Man Cybern. B 39 (6), 1362–1381.